



**HAL**  
open science

## Formulating stable surrogate wood-pyrolysis oil in oil (O/O) emulsions: The role of asphaltenes evidenced by interfacial dilational rheology

Ronald Marquez, Jesús Ontiveros, Véronique Nardello-Rataj, Nicolas Sanson, François Lequeux, Valérie Molinier

### ► To cite this version:

Ronald Marquez, Jesús Ontiveros, Véronique Nardello-Rataj, Nicolas Sanson, François Lequeux, et al.. Formulating stable surrogate wood-pyrolysis oil in oil (O/O) emulsions: The role of asphaltenes evidenced by interfacial dilational rheology. *Chemical Engineering Journal*, 2024, 495, pp.153321. 10.1016/j.cej.2024.153321 . hal-04648132

**HAL Id: hal-04648132**

**<https://hal.science/hal-04648132v1>**

Submitted on 15 Jul 2024

**HAL** is a multi-disciplinary open access archive for the deposit and dissemination of scientific research documents, whether they are published or not. The documents may come from teaching and research institutions in France or abroad, or from public or private research centers.

L'archive ouverte pluridisciplinaire **HAL**, est destinée au dépôt et à la diffusion de documents scientifiques de niveau recherche, publiés ou non, émanant des établissements d'enseignement et de recherche français ou étrangers, des laboratoires publics ou privés.

# 1 Formulating stable surrogate wood-pyrolysis oil in oil (O/O) emulsions: The role 2 of asphaltenes evidenced by interfacial dilational rheology

3 Ronald Marquez\*<sup>1,2</sup>, Jesús F. Ontiveros\*<sup>2</sup>, Véronique Nardello-Rataj<sup>2</sup>, Nicolas  
4 Sanson<sup>1,3</sup>, François Lequeux<sup>1,3</sup>, Valérie Molinier\*<sup>1,4</sup>

5 <sup>1</sup> Laboratoire Physico-chimie des Interfaces Complexes, ESPCI, 10 rue Vauquelin,  
6 75005 Paris, France

7 <sup>2</sup> Univ. Lille, CNRS, Centrale Lille, Univ. Artois, UMR 8181– UCCS – Unité de Catalyse  
8 et Chimie du Solide, 59000 Lille, France

9 <sup>3</sup> Soft Matter Sciences and Engineering, PSL Research University, ESPCI Paris,  
10 Sorbonne Université, CNRS UMR 7615, 10 rue Vauquelin, 75231 Paris Cedex 05,  
11 France

12 <sup>4</sup> TotalEnergies OneTech, Pôle d'Etudes et de Recherche de Lacq, 64170 Lacq, France

## 13 Abstract

14 This work presents a novel methodology to obtain stable bio-oil-in-oil emulsions using  
15 crude oil endogenous asphaltenes as emulsifiers. This approach provides new insights  
16 into the valorization of wood pyrolysis bio-oils through co-processing with crude oils or  
17 by direct incorporation in fuels for marine transportation, contributing to a significant  
18 reduction of the carbon footprint of these products. Similar to water-crude oil systems,  
19 asphaltenes can form a rigid film at the bio-oil / petroleum-derived oil interface, thus  
20 limiting droplets coalescence and increasing the emulsion lifetime without requiring  
21 additional emulsifier. The evolution of the interfacial layers with the asphaltene content  
22 and the nature of the petroleum-derived oil phase were investigated by interfacial  
23 rheology. The results show the consolidation of the interfacial layer and the formation of  
24 a solid-like film, referred to as "skin" with appropriate asphaltene content and polarity of  
25 the oil phase. Changes in the dilational elasticity depend on the asphaltenes  
26 aggregation behaviour according to the Yen-Mullins model, and the mechanisms that  
27 account for these phenomena are discussed.

28  
29 **Keywords:** Bio-oil, Biofuel, Wood pyrolysis oil, Marine fuel, Co-processing, Refinery,  
30 Emulsion, Stability, Asphaltene, Sustainability.

## 31 32 1. Introduction

33 Bio-oils obtained from pyrolysis or hydrothermal liquefaction of wood residues (referred  
34 to as fast pyrolysis bio-oil [1], bio-oil [2], or biocrude [3]) are promising candidates for  
35 incorporation into marine transportation fuels [2] or co-processing with petroleum-  
36 derived oils in refineries [4] due to their reduced carbon footprint [3,5,6]. However, their  
37 complex chemical composition – water, acids, aldehydes, ketones, sugars and lignin  
38 oligomers – renders these bio-oils highly polar and therefore immiscible with  
39 hydrocarbon oils. Moreover, bio-oils can exhibit physical and chemical instability, and  
40 are particularly prone to oxidation and polymerization reactions due to ageing [7,8].  
41 Consequently, solid particle formation, water separation, and incompatibility with crude  
42 oil refinery oils make formulation and use of bio-oils challenging [9].

43 Different alternatives have been proposed to achieve compatibility between bio-oils and  
44 petroleum-derived oils, such as the use of co-solvents to attain miscibility, though this

45 often requires high solvent quantity [10,11]. One alternative method for producing bio-  
46 oil-in-oil emulsions involves the use of surfactants. However, achieving stable oil-in-oil  
47 emulsions typically requires the use of emulsifiers at high concentrations [12–15].  
48 Among the types of emulsifiers used for this purpose are block copolymers, which have  
49 been shown to be effective but costly [16–20]. Hydrodeoxygenation allows the  
50 upgrading of bio-oils to decrease oxygen content, increasing calorific power and  
51 lowering corrosion in engines, yet it is cost-intensive and relies on solid catalysts  
52 [21,22]. Esterification involves converting organic acids (e.g., formic, acetic, and  
53 propionic acid) present in bio-oil into their corresponding esters by reaction with an  
54 alcohol in the presence of catalysts [23–25]. On the other hand, transesterification  
55 substitutes long-chain esters in bio-oil with short-chain alcohols, using solid acid  
56 catalysts to achieve high conversion and selectivity [23]. The latter make bio-oils less  
57 polar and thus partially miscible with petroleum-derived oils, but they are cost-intensive  
58 processes and have only been demonstrated in bench-scale and in some pilot plant  
59 essays [3,6]. Therefore, there is a need to achieve stabilization of blends of wood  
60 pyrolysis bio-oils and petroleum-derived oils, without requiring the addition of chemicals  
61 or the need for bio-oil upgrading. Stabilizing emulsions of such systems requires  
62 understanding the phenomena occurring at the oil/oil interface.

63  
64 Surface rheology has been extensively employed to measure interfacial properties in  
65 oil/water systems with significant advances made in the past two decades in  
66 understanding the behaviour of surface-active species at interfaces. This includes the  
67 adsorption and consolidation of structured monolayers [26,27], emulsion stabilization  
68 [28,29], and the mechanisms behind emulsion instability [30,31].  
69 In interfacial dilational rheology measurements, the dilational modulus can be defined  
70 as (Eq. 1):

71  
72 
$$E = A \frac{d\Pi}{dA} \quad (1)$$

73  
74 where E is the dilational modulus in mN/m (also called compression [32] or dilatational  
75 [29] modulus), A is the surface area in m<sup>2</sup> and  $\Pi$  is the surface pressure in mN/m. For  
76 an insoluble monolayer, the surface surfactant concentration can be expressed as  $\Gamma \sim$   
77  $1/A$  (Eq. 2):

78  
79 
$$E = \Gamma \frac{d\Pi}{d\Gamma} \quad (2)$$

80 At low surfactant concentrations, the surfactant transport to and from the interface is  
81 slow, interfacial dilational parameters are large, and the surface elasticity is orders of  
82 magnitude larger than the surface shear elasticity [27,33]. Therefore, dilational elasticity  
83 measurements are particularly useful to study interfaces, especially when surface-active  
84 species that form aggregates or consolidated structured monolayers are present  
85 [28,32]. In surfactant/oil/water systems at Winsor I or Winsor II conditions, when  
86 agitation and shear occur, generally, a higher interfacial area is available for surfactant  
87 molecules to be adsorbed at the interface [34]. There is evidence that when surface  
88 active macromolecules (such as proteins or asphaltenes) are adsorbed, densification,  
89 molecular rearrangement, and conformation of a rigid film occurs [35,36]. This results in

90 a high value of the dilational modulus and high stability of the emulsions formed  
91 [28,37,38].

92 Marangoni forces are large at low surfactant concentrations when there is not enough  
93 surfactant in the bulk to replenish the surface after a mechanical perturbation. But in  
94 some cases, Marangoni forces remain effective even at high surfactant concentrations  
95 when thin films or insoluble surfactant monolayers are present [27]. This has been  
96 related to a high persistence of the emulsions formed with natural surfactants as  
97 emulsifiers, as in the case of asphaltenes diluted in hydrocarbon solvents [32,39,40], or  
98 proteins [37,41,42] in water-in-oil (W/O) or oil-in-water (O/W) systems, respectively. The  
99 systems mentioned above are based on water/oil systems since there are no reports on  
100 the interfacial rheology of bio-oil/oil systems in the presence of asphaltenes.

101  
102 Several publications indicate that asphaltenes are responsible for the emulsification of  
103 water-in-crude oil emulsions (W/O) due to the formation of a rigid, mechanically  
104 resistant asphaltene film at the interface, as evidenced either by interfacial rheology or  
105 crumpling ratio measurements [28,32,43]. The stability of these asphaltene-stabilized  
106 emulsions has been reported to be affected by the petroleum oil nature. For instance,  
107 diluents with high aromatic content lower the emulsion stability, whereas the paraffinic  
108 oil content increase film elasticity up to the point where the onset of asphaltene  
109 precipitation is reached [43,44].

110  
111 In order to overcome the challenges of compatibilizing bio-oils and petroleum-derived  
112 oils for co-processing applications and as a marine fuel, herein, we explore a promising  
113 approach to obtain homogeneous and stable bio-oil-in-oil emulsions (O/O) using natural  
114 asphaltenes found in crude. We examine the underlying mechanisms behind the  
115 stabilization process in the light of dilational rheology of bio-oil/oil interfacial layers.

## 116 117 **2. Materials and methods**

### 118 119 **2.1 Materials**

120 Decalin (decahydronaphthalene >99%, a mixture of cis-and trans isomers) and  
121 dodecane (>99%) were provided by Sigma-Aldrich. Table 1 lists the purity of all  
122 compounds of the surrogate pyrolysis bio-oil, the density of the mixture is 1.06 g/mL. All  
123 products of Table 1 were provided by Sigma-Aldrich except 2-cyclopentenone that was  
124 provided by Thermo Scientific Acros. Asphaltenes were precipitated from a vacuum  
125 residue ( $^{\circ}\text{API}=12.5$ , SARA: Saturates=26.9, Aromatics=53.6, Resins=15.5,  
126 Asphaltenes=4.0 wt.%, TotalEnergies Gonfreville Refinery, France), using the standard  
127 procedure [45]. **A sample of bio-oil, prepared by fast pyrolysis of pinewood residue  
128 pellets, was provided by TotalEnergies Research and Technology (Gonfreville, France).  
129 The compositional analysis of this bio-oil is reported by Mase et al. [46].**

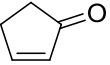
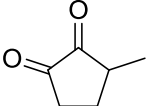
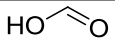
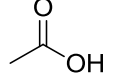
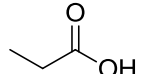
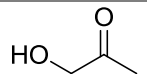
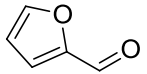
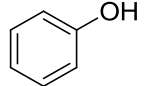
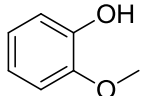
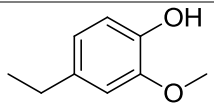
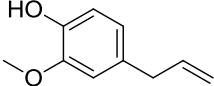
### 130 **2.2 Formulation of a surrogate bio-oil mixture**

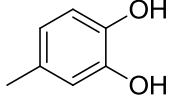
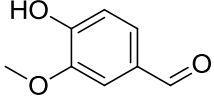
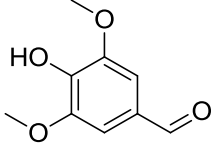
131 Fonts et al. [47] proposed a composition of fast pyrolysis bio-oil by selecting  
132 representative organic compounds based on results analyzed from the literature. This  
133 selection considered: (1) compounds with the higher concentrations in wood pyrolysis  
134 liquids, (2) the presence of compounds from the main chemical families (aldehydes,  
135 ketones, acids, furans, phenols, methoxyphenols, sugars, and oligomers) and

136 containing the most representative functional groups quantified in lignocellulosic  
 137 pyrolysis liquids (carbonyl, carboxyl, phenol OH, and aliphatic OH), (3) the existence of  
 138 compounds typically separated as water-soluble and also water-insoluble, and (4) the  
 139 coverage of the whole range of molecular weights of the compounds present in  
 140 pyrolysis liquids.

141 In the present work, a surrogate bio-oil was obtained as a mixture of the most common  
 142 light constituents of bio-oil by mixing the appropriate quantities of chemical compounds,  
 143 as indicated in table 1. Their structure, purity, Hansen Solubility Parameters and  
 144 average wt.% composition are provided in Table 1. The formulated surrogate bio-oil  
 145 allowed solubilization of water, lignin and sugar components (20, 30, and 20 wt.%,  
 146 respectively) in a homogeneous phase that is stable after three months of observation,  
 147 thus indicating its suitability to represent such complex systems.

148  
 149 **Table 1.** Light compounds within the composition of surrogate fast pyrolysis bio-oil  
 150 proposed by Fonts et al. [47].  
 151

Component	Structure	Purity	Hansen solubility parameters (MPa <sup>1/2</sup> )*			wt. %
			$\delta_d$	$\delta_p$	$\delta_h$	
2-cyclopentenone		98%	18	10.5	7	1.8
3-methyl-1,2-cyclopentanedione		99%	17.2	10.6	7.9	1.8
Formic acid		>95%	16.6	12	15.3	2.9
Acetic acid		>99%	16.1	6.6	10.9	30.6
Propionic acid		>99.5%	16	6.3	10.5	13.3
Hydroxyacetone (acetol)		90-95%	16.6	10.5	13.5	27.1
Furfural		99%	17.5	13	6.2	5.0
Phenol		>99%	18.4	5.8	12.8	3.2
Guaiacol		>99%	18.6	7.1	13.4	1.8
4-ethylguaiacol		>98%	18.2	6.7	12.9	1.4
Eugenol		99%	18.1	6.3	12.4	2.2

4-methylcatechol		>95%	18.9	7.4	19.5	2.9
Vanillin		99%	18.9	11.8	14	5.4
Syringaldehyde		>98%	19	13.1	14.6	0.7

\*Data obtained from HSPiP v.5.4.02

152

153

### 154 2.3 Asphaltenes precipitation

155 100 g of vacuum residue were contacted with 2 L of *n*-heptane (ratio fuel/heptane =  
 156 1/20). The system was agitated for 24 h at room temperature, followed by 24 hours at  
 157 rest. Then, the system was filtered with a PTFE hydrophobic filter (0.2  $\mu\text{m}$ ), and the  
 158 retained asphaltenes were washed several times with *n*-heptane until the filtrate  
 159 became colorless. Subsequently, asphaltenes were dried at 40 °C and ground in a  
 160 mortar. The fuel phases were prepared by redissolving specific amounts of asphaltenes  
 161 in decalin (or a decalin:dodecane 75:25 mixture in wt.%) to reach 0.05, 0.1, 0.5 and 1  
 162 wt.% asphaltenes. In that way, the impact of asphaltene concentration on the emulsion  
 163 stability could be evaluated.

164

### 165 2.4 Formulation of a petroleum-derived oil model system

166 In order to study the role of asphaltenes on the rheology of bio-oil/oil interfacial layers, a  
 167 model system was tailored to obtain bio-oil-in-oil emulsions with varying asphaltene  
 168 content. As a first approach, a low viscosity heptol (*n*-heptane/toluene) hydrocarbon  
 169 mixture phase was considered. However, as shown in Figure S1 (Supplementary  
 170 information), colored components within the bio-oil phase or the surrogate bio-oil phase  
 171 are miscible with low molecular weight hydrocarbons (C7 or lower). This is likely due to  
 172 the compatibility of the low molecular weight components in the bio-oil with the heptol  
 173 phase (for example, heptane and toluene have solubility with acetic acid, which declines  
 174 with higher alkanes [48]). Consequently, a mixture of decalin (cis+trans  
 175 decahydronaphtalene with a Hansen Solubility Parameter  $\delta_d = 17.6$ ) and dodecane ( $\delta_d$   
 176 = 16) was chosen as a model petroleum-derived oil medium that solubilizes asphaltenes  
 177 [49–51], suitable for utilization as a model fuel phase. Decalin as well as dodecane are  
 178 immiscible with surrogate bio-oil and have very low solubility with wood pyrolysis bio-oil  
 179 (Figure S1 Supplementary information, Right panel). **The EACN of crude oils changes**  
 180 **according to its composition and Creton reports values from 6.7 to 18 [52], and according to**  
 181 **Jang et al. [53], it ranges typically from 10-14. Consequently, decalin, a cycloparaffin with**  
 182 **reported EACNs of 5.3 [49,54], known for not inducing asphaltene precipitation, and dodecane,**  
 183 **with a EACN of 12, were selected as hydrocarbon fuel surrogates [54]. Both substances are**  
 184 **immiscible with the bio-oil.**

185

186 **2.5 Emulsion formation**

187 The surrogate bio-oil was pre-heated to 25 °C. The petroleum-derived oil en(decalin or  
188 decalin:dodecane) was also pre-heated at 25 °C and weighed in the same vial. The total  
189 amount of emulsion prepared was 6 g, with the bio-oil constituting 30 wt.% of the  
190 mixture. The vial was sealed and placed in a bath at 25 °C. Then, the bio-oil/petroleum-  
191 based oil mixture was emulsified with a T10 basic Ultra-Turrax at 30,000 rpm for 2  
192 minutes. The emulsion was immediately placed in the Turbiscan apparatus at 25 °C. At  
193 the same time, an emulsion sample was observed at 25 °C with an Olympus BX51  
194 microscope in transmission mode.

195

196 **2.6 Lifetime of emulsions**

197 The stability of the emulsions was continuously monitored using a Static Multiple Light  
198 Scattering (SMLS) Turbiscan Lab Expert (Formulacion, France) at a temperature of 25  
199 °C with measurement intervals of 30 minutes during the first 48 h, followed by every 24  
200 h for 30 days. The transmitted light (T) and backscattered light (BS) were recorded as a  
201 function of the sample height. The collected data were subjected to analysis through the  
202 TurbiSoft Lab software (version 2.3.1.125) [55]. Photographs were taken to evidence  
203 the difference between the lifetime of emulsions with or without paraffines (dodecane  
204 content).

205

206 **2.7 Asphaltenes onset of flocculation**

207 Two sets of experiments were conducted to study the impact of the solvent medium on  
208 the flocculation behavior of asphaltenes. Static Multiple Light Scattering (SMLS) was  
209 used to obtain the transmission and backscattering profiles of the samples as a function  
210 of time, and dynamic light scattering (DLS) was used to assess the asphaltene particle  
211 size distribution. The concentrations studied were 0.05 wt.% asphaltenes and  
212 dodecane/decalin mixtures with 0, 30, 40, 50, 60, 80 and 100 wt.% dodecane. SMLS  
213 measurements were performed every hour for 5 days using the methodology described  
214 in section 2.6. DLS measurements were conducted 30 days after the samples were  
215 mixed, to attain complete sedimentation of the precipitated asphaltenes. Liquid was  
216 taken from the top of the sample, added to a quartz cuvette, and the particle size  
217 distribution was measured at 25 °C using a Zetasizer (Nano ZS ZEN 3600, Malvern,  
218 UK) equipped with a He-Ne laser at 632.8 nm. The Zetasizer ZS measures the  
219 scattering information at 173°, which is the angle of maximum backscattering intensity  
220 for small particles [56]. The size distribution of asphaltene aggregates in the sample  
221 was calculated by using the Stokes-Einstein equation, which relates the particle size to  
222 the diffusion coefficient [57]. Additionally, visual observation was used to follow  
223 asphaltene precipitation after a 30-day ageing period (Figure S2 Supplementary  
224 Information), thus confirming the results obtained by SMLS and DLS.

225

226

227 **2.8 Interfacial dilational rheology measurements with the pendant drop technique**

228 Interfacial tension and interfacial dilational rheology measurements were performed on  
229 a bio-oil (or surrogate bio-oil) / decalin system with varying asphaltene content.  
230 Interfacial properties were measured by changing asphaltene concentration in the  
231 hydrocarbon phase. A drop profile tensiometer (Teclis, France) was used to measure

232 the variation of dilational rheology of the interfacial layer throughout the scan. The  
233 hydrocarbon phase nature was also changed by using a decalin:dodecane mixture. The  
234 asphaltene concentration scan was performed between 0 and 1 wt.% asphaltenes in the  
235 case of decalin solvent, and between 0 and 0.15 wt.% when a 75 vol.% decalin and 25  
236 vol.% dodecane solvent mixture was used. In the latter case, concentrations up to 0.15  
237 wt.% asphaltenes were measured, because at higher values, the asphaltene film  
238 evolved very rapidly and a non-Laplacian shape droplet was formed in around one  
239 minute. Dynamic interfacial tension and interfacial dilational rheology properties were  
240 determined by placing the transparent phase in the cuvette and the darker phase in the  
241 syringe, which was injected through the needle. A drop of oil of the darker phase with a  
242 volume of 1-2  $\mu\text{L}$  was formed at the tip of the needle. A pendant or rising drop  
243 configuration was used according to the density difference between the two phases.  
244 According to Hutin et al. [58,59] both methods have been shown to be suitable for the  
245 measurement of interfacial tension and interfacial rheology of asphaltene-laden  
246 interfaces. A viscoelastic and highly mechanical resistant film (which has been  
247 previously referred to as “skin”) was rapidly formed in all systems (in less than 20 min).  
248 The interfacial tension and area were determined in the drop profile equipment through  
249 axisymmetric drop shape analysis [60]. The drop area can be varied sinusoidally with  
250 oscillatory changes in the drop volume, leading to an oscillatory change in drop area  
251 and interfacial tension through the dilatation and expansion of the drop.

252  
253 In viscoelastic interfaces, variations in interfacial tension and interfacial area, measured  
254 at a frequency  $\omega$ , lead to a difference in the phase, accounted for by the phase angle  $\varphi$ .  
255 The phase angle quantifies the difference in degrees between both the interfacial  
256 tension and interfacial area sinusoidal curves, i.e.,  $\varphi = 0^\circ$  corresponds to a totally elastic  
257 response, while  $\varphi = 90^\circ$  indicates a completely viscous response. An interface with an  
258 intermediate phase angle between  $0^\circ$  and  $90^\circ$  is considered viscoelastic, and two  
259 contributions are necessary to describe it, the storage  $E'$  and the loss  $E''$  modulus (also  
260 known as elastic and viscous moduli, respectively). The dilational modulus can be  
261 expressed as a complex number that considers both contributions (Eq. 3):

$$262$$
$$263 \quad E = E' + iE'' \quad (3)$$
$$264$$

265  $E'$  and  $E''$  account for the energy stored and the energy dissipation through relaxation  
266 processes, respectively. They can be obtained from the phase angle through equations  
267 (4) and (5):

$$268$$
$$269 \quad E' = E \cos(\varphi) \quad (4)$$

$$270 \quad E'' = E \sin(\varphi) \quad (5)$$
$$271$$

272 In this work, dilational elasticity experiments were tailored for a variation of interfacial  
273 area of less than 10% (to maintain the rheological response linear) by controlling the  
274 drop volume amplitude. The frequency of oscillation of surface area was generally set to  
275 0.1 Hz. In addition, oil phases densities were measured in a pycnometer. The  
276 corresponding errors range from 2 to 5% for interfacial tensions and from 4 to 10% for  
277 the dilational modulus. All experiments were conducted at a temperature of  $20 \pm 2^\circ\text{C}$ .



278 Teflon-coated needles (Teclis, France), ranging in size from 0.5 to 2 mm, were selected  
279 based on the viscosity of the liquids and the interfacial tension. Additionally, all  
280 experiments were performed with a Bond number above 0.1. To ensure repeatability,  
281 at least three experiments were conducted for each condition.

282

## 283 2.9 Crumpling ratio

284 The crumpling ratio is a measure of the relative area reduction at which a crumpling  
285 phenomenon occurs on the surface of a drop, leading to surface roughness due to  
286 apparent buckling. This phenomenon is attributed to the formation of a rigid skin at the  
287 surface and typically occurs during the retraction of the volume inside a droplet that has  
288 been contacted with an asphaltene-rich phase. Above a certain reduction of area,  
289 named “crumpling point,” the relative area reduction is defined as the crumpling ratio  
290 with equation (6) [28]:

291

$$292 \text{ Crumpling ratio} = \frac{A_{final}}{A_{initial}} \quad (6)$$

293

294 where  $A_{initial}$  is the initial droplet area and  $A_{final}$  is the area when “crumpling” occurs.

295

296 The crumpling ratio was measured using a Tracker pendant drop apparatus. An oil drop  
297 with a volume of 1  $\mu\text{L}$  was formed and retracted at a constant rate of 0.1  $\mu\text{L/s}$ . The drop  
298 retraction (and consequent compression of the “skin”) was carried out after the two  
299 phases had been in contact for 3-5 min to allow for stabilization of the interfacial tension  
300 value.

301

## 302 3. Results and discussion

303

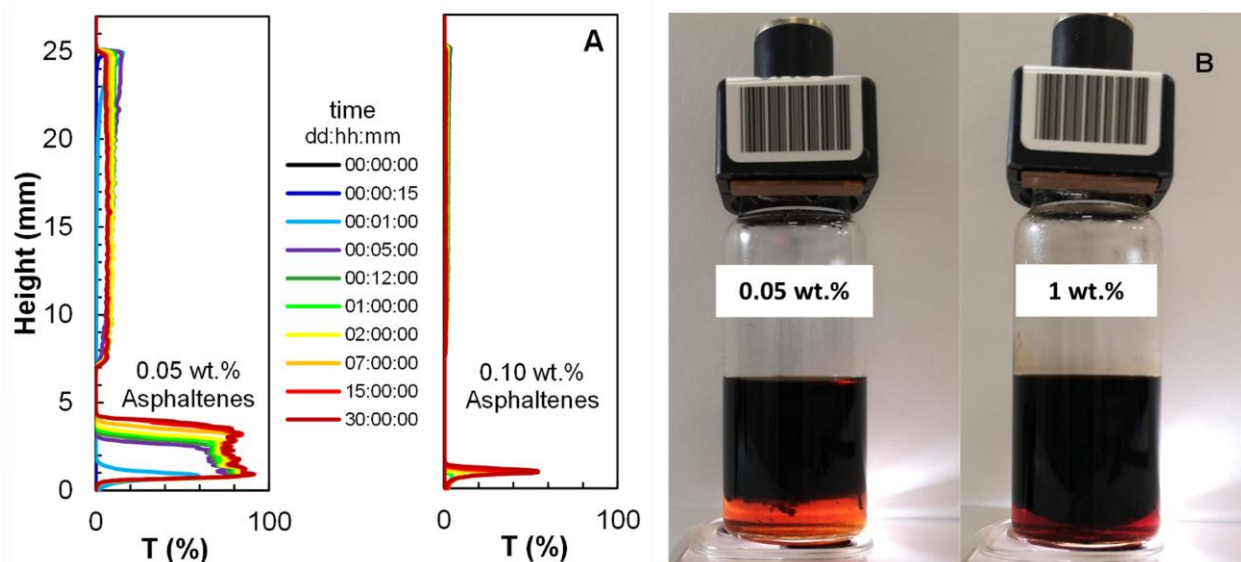
### 304 3.1 Surrogate bio-oil in oil emulsions

305 The polar character of pyrolysis bio-oil makes it immiscible with typical hydrocarbon oils.  
306 In this work, the petroleum-based oil was a reconstituted fuel, obtained by adding  
307 asphaltenes to a decalin or decalin/dodecane mixture, to attain asphaltene  
308 concentrations of 0, 0.05, 0.1, 0.5, and 1 wt.%. Emulsions of the surrogate oil in the  
309 asphaltene-hydrocarbon solution were formulated according to the described  
310 methodology.

311

312 In Figure 1A, the transmission profiles show that emulsions at 0.05 wt.% asphaltenes in  
313 decalin are highly unstable. Since the density of the surrogate bio-oil is higher than that  
314 of decalin, any change in transmission at the bottom of the tube can be interpreted as  
315 coalescence (while a change at the top of the tube would indicate sedimentation).  
316 Within 5 hours, the transmission increases significantly and nearly reaches an  
317 asymptotic value that persists for one month. When the concentration is increased to 1  
318 wt.% (Figure 1B) stability increases but coalescence still occurs. Turbiscan profiles for  
319 concentrations greater than 0.1 wt.% are **ineffective** because asphaltenes provides a  
320 black color to the system, which renders transmission and backscattering signals not  
321 useful to determine changes in the tubes, that is why we provide 0.1 wt.% for turbiscan  
322 measurement but 1 wt.% asphaltenes in Figure 1B for illustration. To monitor  
323 destabilization, a light in the bottom of the sample must be used as shown in the

324 photographs of Figure 1B. These pictures at 30 days demonstrate that increasing  
325 asphaltenes concentration enhances stability, although complete stability is not attained  
326 in this case even at 1 wt. % asphaltenes. Thus, the effect of adding a component with a  
327 paraffinic nature is crucial to obtain stable emulsions as will be shown in Figure 2. As in  
328 typical W/O emulsions found in petroleum industry, asphaltenes also appear to stabilize  
329 the polar surrogate bio-oil droplets in decalin. The higher stability of surrogate bio-oil-in-  
330 oil emulsions at asphaltene concentrations above 0.5 wt.% suggests the potential use of  
331 petroleum surface active species (*i.e.*, asphaltenes), which are present in some fuel  
332 phases as emulsifiers.  
333

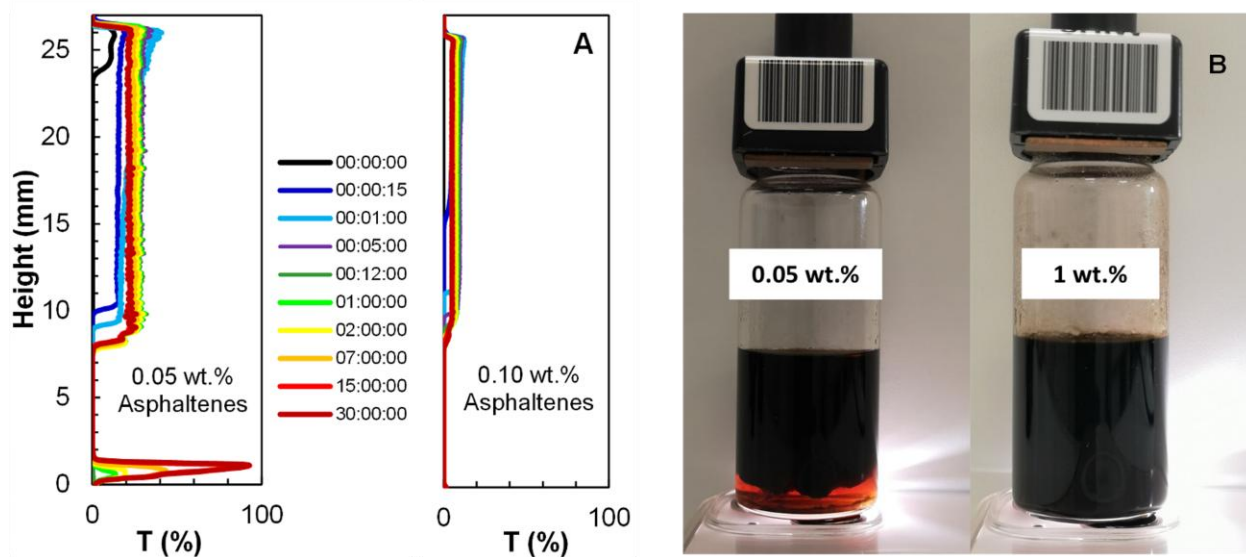


334 **Figure 1.** A) Static multiple light scattering separation profiles measured using the  
335 turbiscan through 30 days. The samples are surrogate bio-oil in decalin emulsions at  
336 0.05 and 0.1 wt.% of asphaltene. T = 25 °C. B) Photography of 0.05 and 1 wt.%  
337 emulsions after 30 days. Turbiscan measurements are presented up to 0.1 wt.%  
338 asphaltenes because over 0.2 wt.% the top oil phase does not transmit light, and the  
339 bottom phase becomes darkened.  
340

341  
342 In order to study the influence of the nature of the oil phase containing the asphaltenes,  
343 surrogate bio-oil was emulsified in a decalin:dodecane (75:25) mixture at the same  
344 asphaltenes concentrations. The decalin:dodecane 75:25 mixture was selected  
345 because it is a combination of cyclic and linear alkanes (the first one being a suitable  
346 solvent for asphaltenes, while the second one is not due to the long chain length). This  
347 was done aiming to find a model oil similar to heptane:toluene 25:75 mixtures (heptol),  
348 which have been utilized as surrogate oil to study the interfacial rheology of asphaltene  
349 containing systems [28,32,44]. Figure 2A shows the transmission profiles for 0.05 and  
350 0.1 wt.% of asphaltenes in the decalin:dodecane mixture. Analogous to the decalin  
351 systems, increasing the asphaltene concentration improves the stability of the system.  
352 The photographs of the emulsions show that, this time, the system at 1 wt.%  
353 asphaltenes remains stable at 30 days. Visual and microscopic inspection evidence  
354 large lifetimes. Comparing both figures, it can be noted that although both emulsions

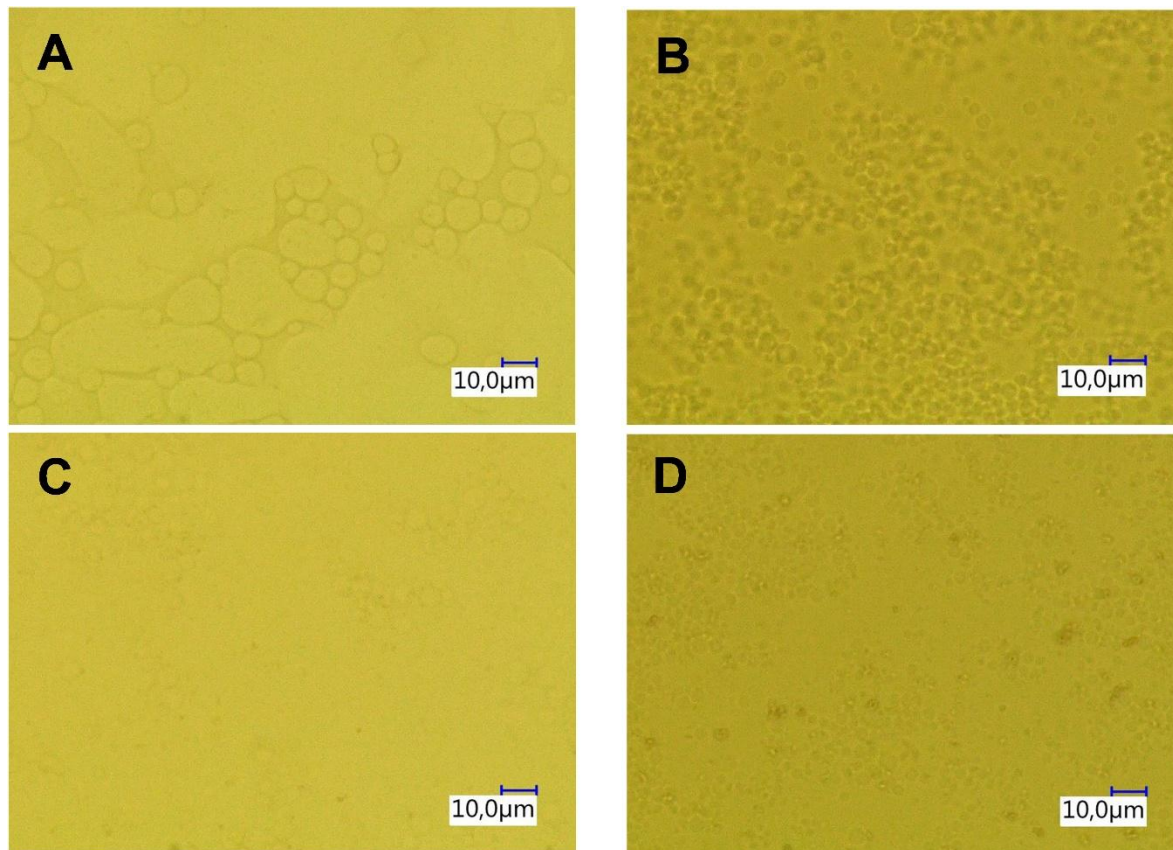
355 are unstable at 0.05 wt.%, the coalescence rate is lower for the decalin:dodecane  
356 mixture and the coalescence starts only after 24 hours. Emulsions above 0.2 % remain  
357 stable over two months when dodecane is added. **Figure 3 shows microphotographs of**  
358 **the emulsions. Emulsions A and B have decalin as a hydrocarbon solvent medium and**  
359 **are unstable after a lifetime of 10 minutes, evidenced by an increase in droplet size due**  
360 **to coalescence. Emulsions C and D have a mixture decalin/dodecane = 0.75/0.25 as**  
361 **external phase and remain stable during the observation time of 10 min, with emulsion**  
362 **D displaying a particularly small droplet size. Therefore, asphaltene concentration as**  
363 **well as the oil's paraffin content are critical factors in achieving stable bio-oil-in-oil**  
364 **emulsions.** This contributes to understanding the stabilization phenomena likely  
365 involved. Multiple reports in the literature indicate that asphaltenes are responsible for  
366 the emulsification of water-in-crude oil emulsions due to the formation of a rigid  
367 asphaltene film at the interface [28,32,44]. The stability of emulsions has been reported  
368 to be affected by the nature of the oil medium, asphaltenes interfacial activity,  
369 aggregation, and precipitation, which is related to the hydrocarbon solvent in which they  
370 are dispersed [28,32,44,61]. For instance, diluents with high aromatic content decrease  
371 the emulsion stability, whereas the presence of paraffinic oil makes the film more rigid  
372 until the onset of asphaltene precipitation is reached [28,32,44].

373  
374 Moreover, recent research has linked these phenomena to the Hansen Solubility  
375 Parameter of the solvent [51]. Accordingly, in the present research the solvent is varied  
376 from pure decalin to a dodecane:decalin (25:75) mixture, which is revealed by the  
377 change of the Hansen Solubility Parameter  $\delta$  from 17.6 to 17.2 MPa<sup>1/2</sup>. This indicates a  
378 shift towards a less polar medium when dodecane is added. When comparing their  
379 equivalent alkane carbon number (EACN), a measure of the hydrophobicity of the oils,  
380 the EACN for decalin is 5.3 [49,62], while dodecane is 12. The EACN of  
381 dodecane/decalin mixture is thus higher than for decalin, indicating that decalin is less  
382 hydrophobic.



383 **Figure 2.** A) Static multiple light scattering separation profiles of surrogate bio-oil in oil  
384 emulsions measured with the Turbiscan through 30 days. The solvent medium is a  
385

386 mixture of decalin:dodecane 75:25 at 0.05 and 0.1 wt.% of asphaltenes. T = 25 °C. B)  
387 Photography of 0.05 and 1 wt.% emulsions after 30 days. Turbiscan measurements are  
388 presented up to 0.1 wt.% asphaltenes because over 0.2 wt.% the top oil phase does not  
389 transmit light, and the bottom phase becomes darkened.  
390



391 **Figure 3.** Emulsified systems at a surrogate bio-oil/oil ratio 30/70. Photographs were  
392 taken after a lifetime of 10 minutes. A) 0.5 wt.% asphaltenes, decalin as oil; B) 1 wt.%  
393 asphaltenes, decalin as oil; C) 0.5 wt.% asphaltenes, decalin/dodecane = 0.75/0.25; D)  
394 1 wt.% asphaltenes, decalin/dodecane = 0.75/0.25.  
395  
396

397 These results provide preliminary guidelines to formulate fuels with high emulsifying  
398 performance for bio-oils by adding saturates-rich or paraffinic phases before the  
399 asphaltene onset of precipitation occurs. The relationship between  $\delta_{HSP}$  parameter and  
400 emulsion stability has been recently reported for water-in-crude oil emulsions stabilized  
401 by asphaltenes, *i.e.*, more polar solvents decrease asphaltene emulsifying efficacy and  
402 can break emulsions [63]. **It is essential to highlight the novelty of the present research;**  
403 **this is the first time that such stable bio-oil-in-fuel emulsions, stabilized by asphaltenes**  
404 **(*i.e.*, without any synthetic surfactants or emulsifiers), are reported.** To verify the present  
405 hypothesis, the results of asphaltene solubility in the decalin/dodecane oil are presented  
406 in the next section.  
407



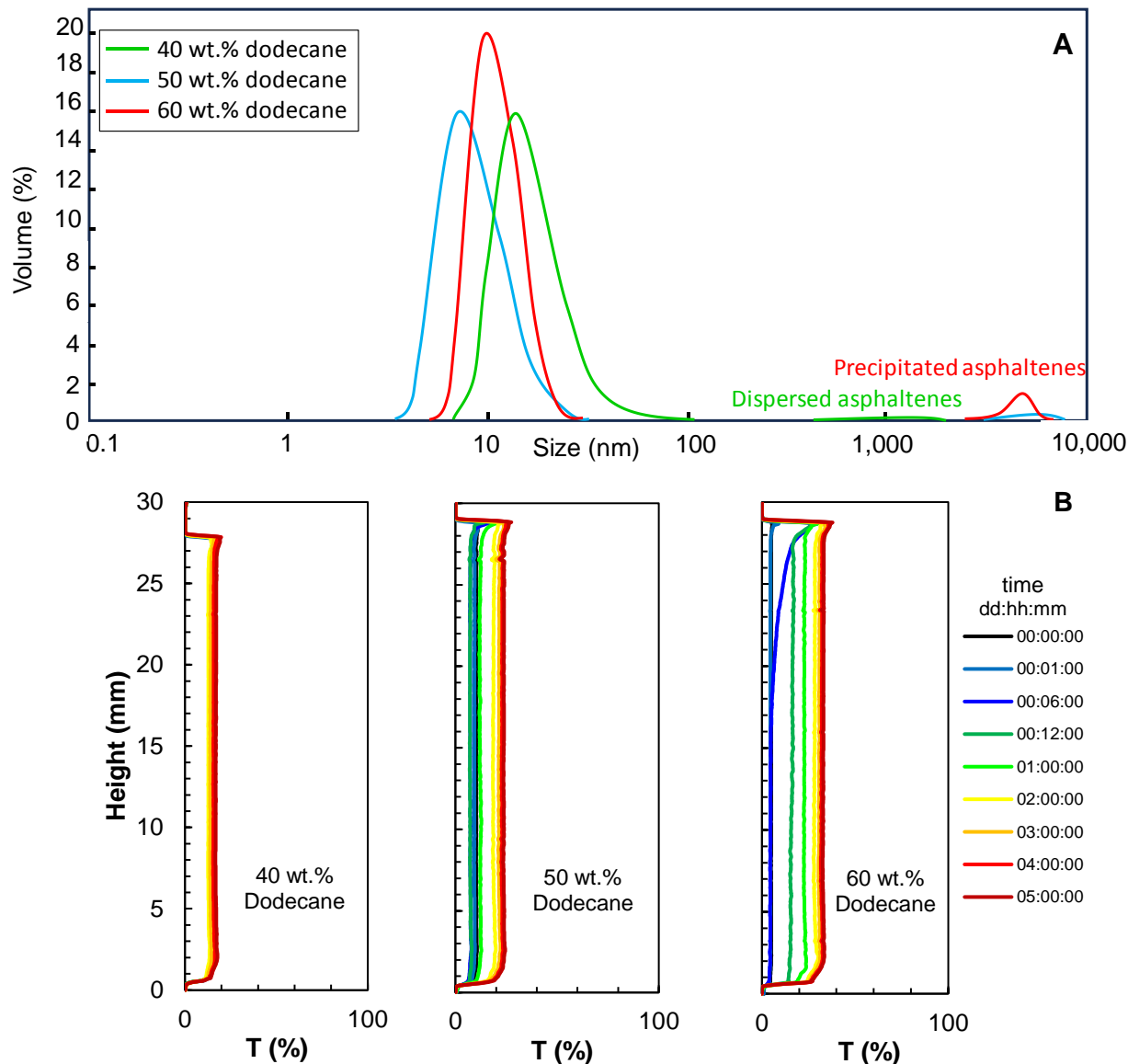
### 408 **3.2 Aggregation of asphaltenes in decalin/dodecane oil systems**

409 Decalin is a suitable solvent for asphaltenes, while dodecane, a linear paraffinic oil,  
410 leads to asphaltenes precipitation. The addition of dodecane to decalin increases the  
411 activity of asphaltenes at the interface, up to the flocculation point, a phenomenon which  
412 has been extensively shown in the literature for water/oil interfacial layers [28,44,64].

413 In the present work, a study of the asphaltenes onset of precipitation in petroleum-  
414 derived oils was performed by adding dodecane to decalin until the onset of  
415 precipitation was attained (See Figure S2 in the supplementary information). The onset  
416 of flocculation was found at 50 wt.% dodecane by visual observation (modified ASCI  
417 [65]), by changes in the transmission and backscattering profiles with the Turbiscan  
418 measurements, and changes in the aggregate size determined by dynamic light  
419 scattering (DLS). Figure 4A illustrates that the average size of asphaltene particles in  
420 decalin at low dodecane concentrations ranges from 8 to 12 nm, but progressively  
421 increases with the addition of dodecane until their precipitation starts when aggregates  
422 are around  $> 5 \mu\text{m}$ . Moreover, according to the literature, the bimodal particle  
423 distribution that occurs between 40 and 60 wt.% dodecane, corresponds to  
424 nanoaggregates and cluster aggregation states [66,67]. The Yen-Mullins model predicts  
425 that asphaltene aggregates can range in size from nanometers to micrometers, with the  
426 larger aggregates being more prevalent in heavier crude oils [68,69]. However, the  
427 exact size of asphaltene aggregates is difficult to measure experimentally, and there is  
428 still ongoing research to better understand the size and structure of these aggregates.  
429 Figure 4B shows the transmission profiles for the same samples as Figure 4A. As the  
430 proportion of dodecane increases, the change of the transmission profile evolves faster  
431 over time. At 40% dodecane, the change in transmission over time is almost negligible,  
432 but at 60 wt.% dodecane, the evolution with time is evident, indicating **aggregation**  
433 phenomenon. Indeed, the “end” values of the transmission profile are higher for the 60  
434 wt.% dodecane than for the **other** two samples because the solvent contains  
435 **aggregated** asphaltenes, increasing light transmission.

436  
437 These results indicate that asphaltenes in a solvent medium with increased paraffin  
438 content are more effective for stabilizing emulsions. On the one hand, asphaltenes in  
439 decalin are very stable and do not separate within 5 days of observation. On the other  
440 hand, the system with 25 wt.% dodecane is closer to the asphaltene onset of  
441 precipitation and exhibits higher emulsification performance, as evidenced by the lower  
442 quantity of asphaltenes required to obtain a stable emulsion i.e., when Figure 1 is  
443 compared to Figure 2.

444



445  
446  
447 **Figure 4.** A) Dynamic multiple and B) static light scattering separation profiles  
448 measured with the turbiscan and DLS apparatus. The solvent medium is a mixture of  
449 decalin:dodecane at increasing wt.% of dodecane with 0.05 wt.% asphaltenes. T = 25  
450 °C.

### 451 3.3 Dynamic Interfacial properties of oil / oil systems with asphaltenes

#### 452 3.3.1 Asphaltenes at Surrogate bio-oil/decaline interfaces

453  
454  
455 Similar to the challenges encountered in Turbiscan measurements, measuring  
456 interfacial tension and dilational rheology of the surrogate bio-oil and hydrocarbons  
457 interfaces is complicated. This is due to the formation of a pendant bio-oil drop in a  
458 decalin/dodecane medium at high asphaltene content, which is black and opaque,

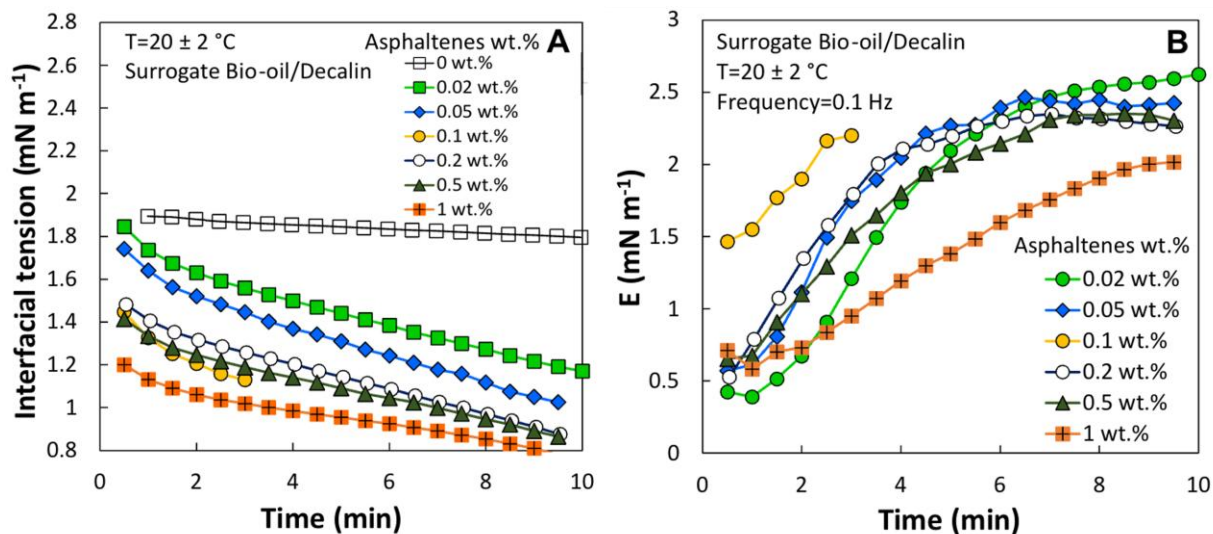
459 thereby impeding light transmission. Even if this configuration resembles the bio-oil  
460 droplet in the decalin/dodecane continuous phase of emulsions, the only practical way  
461 to quantify these properties is to use a translucent surrogate bio-oil medium with a  
462 decalin/dodecane drop in a rising drop configuration. This setup allows a favorable  
463 visualization for performing dilational rheology measurements. In Figure 5 and Figure 6,  
464 the interfacial rheology of decalin with asphaltene content (drop)/surrogate bio-oil (bulk  
465 phase) system is shown.

466  
467 Figure 5A displays the dynamic interfacial tension (IFT) measured for systems from  
468 0.02 to 1 wt.% asphaltenes. An IFT of 1.9 mN/m is measured for the system without  
469 asphaltenes under oscillation. The application of sinusoidal area variation does not alter  
470 the IFT, indicating the absence of substances with interfacial activity. The IFT  
471 decreases over time for all systems containing asphaltenes, and shows lower values as  
472 the asphaltene concentration increases, similar to water/petroleum-based oil interfaces,  
473 albeit with much lower values [35,44]. The increase of the concentration of asphaltenes  
474 slightly reduces the interfacial tension until it exhibits an asymptotic behavior (note that  
475 values of IFT at 0.5 and 1% wt. are almost identical at 10 minutes). This occurs  
476 because the interface is aged and a solid-like film forms around the droplet (where  
477 crumpling occurs), and a non-Laplacian droplet shape is attained, thus impeding a  
478 correct measurement under oscillation.

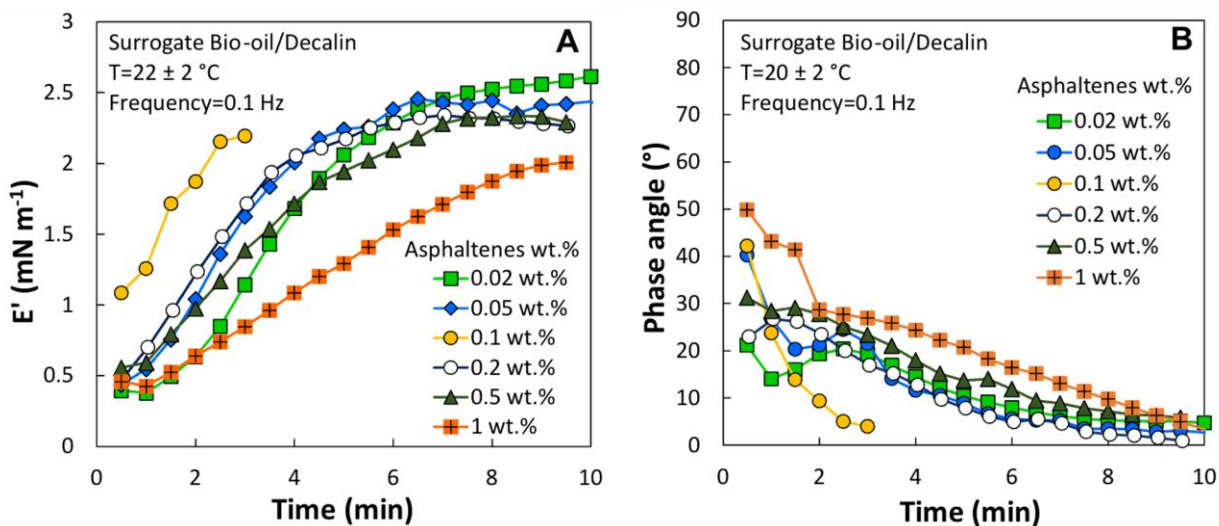
479  
480 IFT values below 2 mN/m and a dilational modulus ( $E$ ) around 0.5-2.5 mN/m for a bio-  
481 oil/petroleum-based oil with an asphaltene film represent the first report of an interfacial  
482 tension and dilational modulus of an oil/oil interface in a drop profile setup. The  
483 decalin/surrogate bio-oil oscillation experiments without asphaltenes did not show any  
484 response to oscillation, resulting in a dilational modulus around zero, as expected [32].  
485 Figure 5B shows that  $E$  increases with the droplet ageing over time. After 3 minutes, the  
486  $E$  value for a 0.1 wt.% asphaltene content is approximately four times greater than that  
487 of the system with 0.02 wt.% asphaltenes. **Moreover, the droplet shape at 0.1 wt.%  
488 becomes non-axisymmetric at 3 min, probably due to the rapid formation of a so-called  
489 "skin". In oil/water interfaces with asphaltene content the non-axisymmetric shape is  
490 attained usually after 30 min of measurement. In the present case, the evolution of the  
491 interfacial tension and  $E$  is fast, probably due to accelerated dynamics of adsorption of  
492 interfacially active species at low interfacial tensions [30,32].** Unlike the interfacial  
493 tension tendency, the dilational modulus reaches a maximum as the asphaltenes  
494 concentration increases. At 0.1 wt.% asphaltenes,  $E$  is higher initially (<3 minutes) than  
495 at other concentrations, and a non-Laplacian droplet shape forms rapidly, indicating the  
496 formation of a solid-like interfacial film.

497  
498 The evolution of asphaltene interfacial layers is evidenced in Figure 6, where  $E'$   
499 increases and phase angle decreases with time, indicating the formation of a solid-like  
500 asphaltene layer. This suggests that a solid-like asphaltene layer at the interface is  
501 responsible for the high stability of previously shown emulsions.

502



503  
 504 **Figure 5.** Interfacial dilational rheology of decalin with asphaltene content (rising drop)  
 505 in surrogate bio-oil at 0.02–1 wt.% asphaltenes. A) Dynamic interfacial tension. B)  
 506 Evolution of the dilational modulus ( $E$ ) while ageing, obtained with oscillatory  
 507 measurements at constant frequency of 0.1 Hz. At 0 wt.% asphaltenes (surrogate bio-  
 508 oil/decalin), IFT = 1.9 mN/m and  $E = 0$  mN/m, with no interfacial rheology response  
 509 when the droplet is subjected to area oscillation, indicating that there are no substances  
 510 with interfacial activity.  $T=20 \pm 2$  °C. The measurements are shown for 10 minutes  
 511 because at larger times a non-Laplacian shape was attained, and  $E$  measurement  
 512 under oscillation could not be performed.  
 513



514  
 515 **Figure 6.** Dilational rheology of decalin (0.02-1 wt.% asphaltenes) / surrogate bio-oil  
 516 interfaces during ageing. A) Evolution of the elastic modulus ( $E'$ ) as a function of time.  
 517 B) Phase angle ( $\phi$ ) as a function of time. Measurements were obtained with oscillatory  
 518 measurements at constant frequency of 0.1 Hz.  $T = 20 \pm 2$  °C. The measurements are  
 519 shown for 10 minutes because at larger times a non-Laplacian shape was attained, and  
 520  $E$  measurement under oscillation could not be performed.  
 521

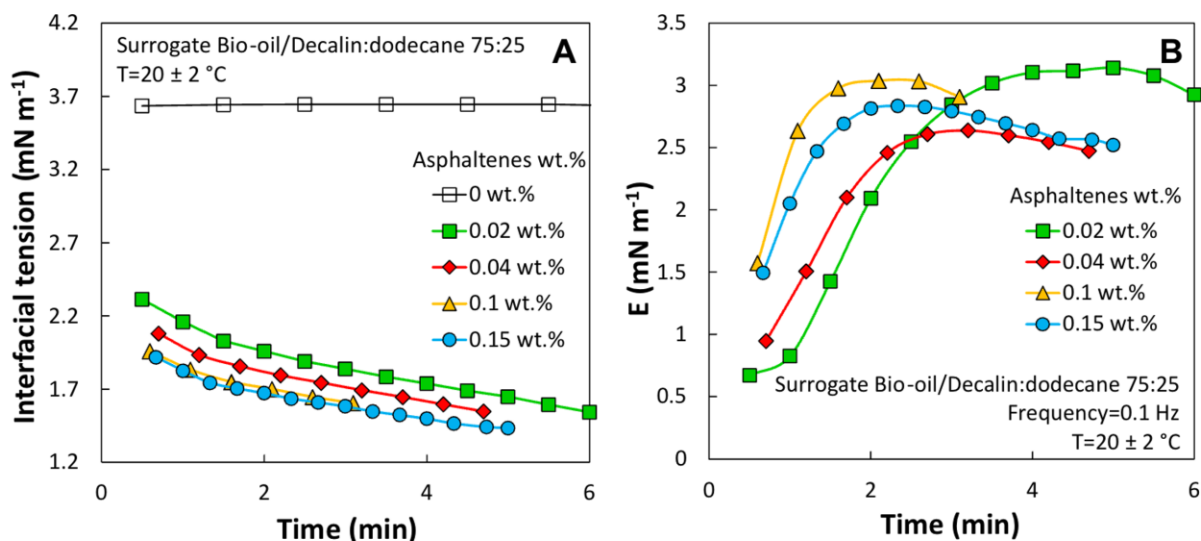


522 Analogously to results in figure 6B, and as previously reported for asphaltenes in heavy  
523 oil/water interfaces [28],  $E'$  presents a maximum value in figure 6A at 0.1 wt.%  
524 asphaltenes. At this concentration the phase angle decreases very fast, showing a  
525 faster evolution of the interfacial layer during ageing.

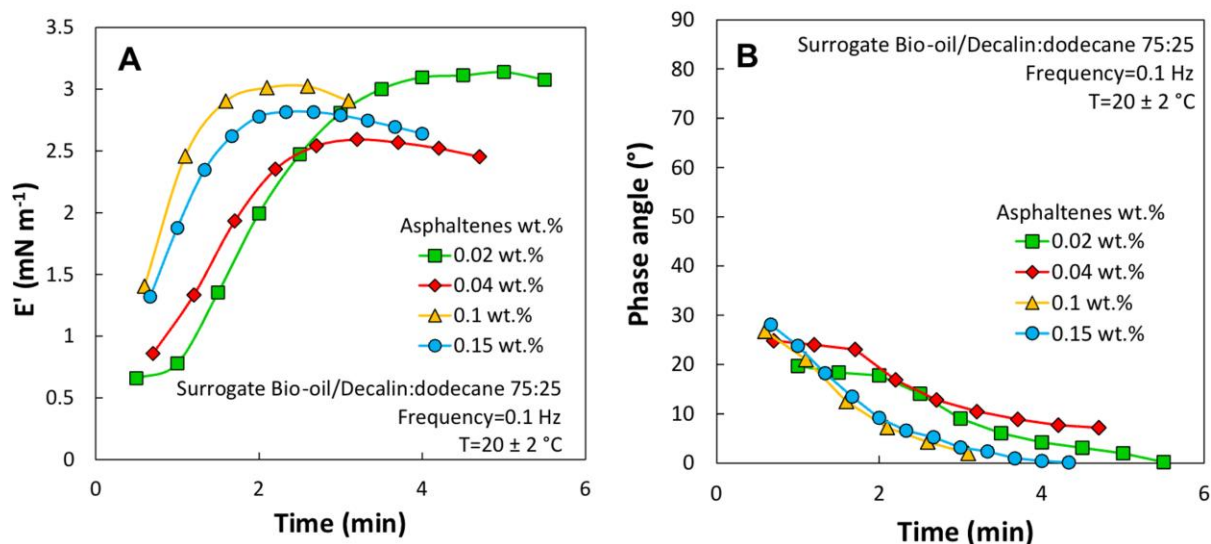
526  
527

### 3.3.2 Asphaltenes at Surrogate bio-oil/decalin:dodecane interfaces

528 In Figures 7 and 8, the interfacial rheology of a decalin:dodecane 75:25 (drop)/surrogate  
529 bio-oil (bulk) system is presented. These findings corroborate the previous results  
530 observed in decalin systems, characterized by a decreasing IFT and an increasing  $E'$ ,  $E''$   
531 and lower phase angle as the asphaltene content increases. Similar to the decalin  
532 system, at 0.1 wt.% asphaltenes a maximum in  $E'$  is attained. In this case, the interfacial  
533 “skin” evolves and consolidates very fast (in less than 2 min), highlighting the effect of  
534 the dodecane addition on the asphaltenes adsorption at the interface. Consequently, a  
535 plateau in  $E$  is reached once the “skin” forms around the droplet, resulting in a non-  
536 Laplacian droplet shape. Systems with asphaltene concentration up to 0.15 wt.% were  
537 measured, beyond this value the “skin” ages very fast and a non-Laplacian droplet is  
538 formed in less than 2 min. Crumpling ratios are a suitable measurement to evidence  
539 such systems with “skin” formation and will be discussed in the next section.



540  
541 **Figure 7.** Interfacial dilational rheology of decalin:dodecane 75:25 with asphaltene  
542 content (rising drop) in surrogate bio-oil at 0.02 – 0.15 wt.% asphaltenes. At 0 wt.%  
543 asphaltenes (surrogate bio-oil/decalin), IFT = 3.6 mN/m and  $E = 0$  mN/m, with no  
544 interfacial rheology response. A) Dynamic interfacial tension. B) Dilational modulus ( $E$ )  
545 obtained with oscillatory measurements at constant frequency of 0.1 Hz.  $T = 20 \pm 2 \text{ }^\circ\text{C}$ .  
546 The measurements are shown for 6 minutes because at larger times a non-Laplacian  
547 shape was attained, and  $E$  measurement under oscillation could not be performed.



548  
 549 **Figure 8.** Interfacial dilational rheology of decalin:dodecane 75:25 with asphaltene  
 550 content (rising drop) in surrogate bio-oil at 0.02 – 0.15 wt.% asphaltenes. A) Evolution of  
 551 the elastic modulus ( $E'$ ) as a function of time. B) Phase angle ( $\varphi$ ) as a function of time.  
 552 Measurements were obtained with oscillatory measurements at constant frequency of  
 553 0.1 Hz.  $T=20 \pm 2$  °C. The measurements are shown for 6 minutes because at larger  
 554 times a non-Laplacian shape was attained, and  $E$  measurement under oscillation could  
 555 not be performed.

556  
 557 In order to take a closer look at this phenomenon, in Figure 9, the values of IFT and  $E$   
 558 are shown as a function of asphaltene content, measured at 3 min of interface ageing.  
 559 IFT decreases with asphaltene concentration, due to the aggregation of asphaltenes in  
 560 petroleum-based oils and their adsorption at the interface, which have been reported in  
 561 the literature for water/petroleum-derived oil systems [28,44]. On the other hand, a  
 562 maximum in  $E$  is found around 0.1 wt.% asphaltenes. This phenomenon has been  
 563 associated with asphaltene aggregation and the formation of a 3D interfacial film for  
 564 water/crude oil systems [28,35,70], and the novelty of the present research is that such  
 565 evidence is presented for a bio-oil/oil system. Afterward,  $E$  and  $E'$  decrease, which has  
 566 been related to the 3D film formation.

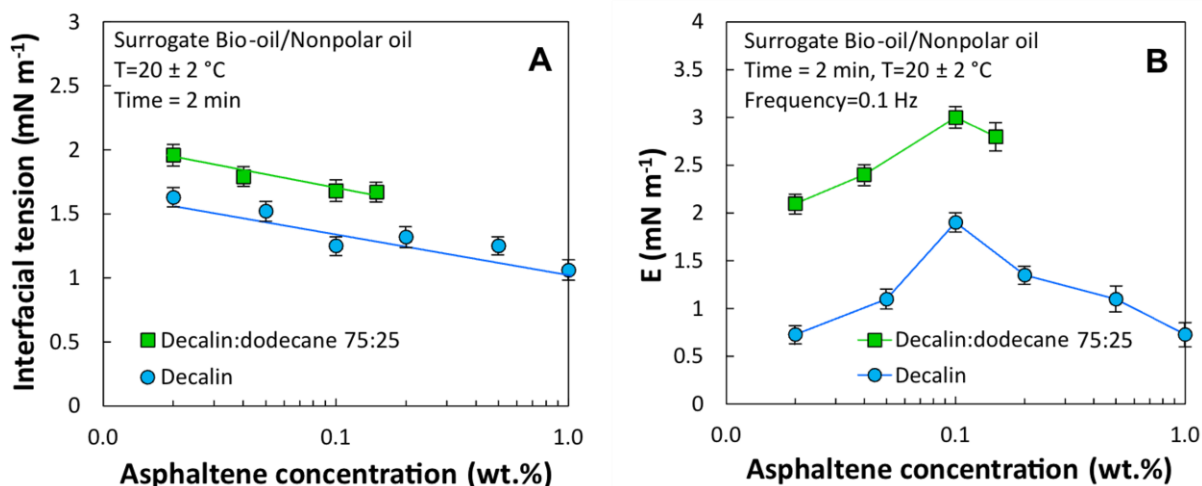
567  
 568 There is limited research regarding the behavior of bio-oil/oil systems with asphaltenes  
 569 content; however, significant research on oil/water systems containing asphaltenes  
 570 exists due to their relevance in petroleum production, particularly concerning stable  
 571 water-in-oil emulsions and demulsifier efficacy [35]. We observe a maximum in the  
 572 modulus  $E'$  and the crumpling ratio, a behaviour documented by Alvarez et al. [28] and  
 573 Goual et al. [71] for asphaltenes at interfaces. This transition results in the formation of  
 574 a “skin” on the pendant drop equipment around the droplet, leading to the formation of  
 575 non-Laplacian shapes, which the equipment cannot accurately measure [28,71,72].

576  
 577 Alvarez et al. [72] noted that the diameter of asphaltene aggregates correlates with the  
 578 thickness of the interfacial layers, suggesting that the maximum in  $E'$  corresponds to a  
 579 structural shift from a 2D to a 3D interfacial layer configuration. This 3D layer provides

580 protection to the emulsion droplets against coalescence [32]. At low asphaltene  
581 concentrations, the adsorbed layer exhibits "crumpling" under compression, a  
582 phenomenon that is absent above certain concentration thresholds. One argument  
583 given to explain the maximum of the dilational modulus was due to a structural transition  
584 and a change in composition of the adsorbed layer. It has been discussed that the  
585 interfacial layer remained smooth above the transition, regardless of the degree of  
586 reduction in surface area [28,71].

587  
588 Thus, reorganization and consolidation of the asphaltene film could be responsible for  
589 interfacial related phenomena such as emulsion stabilization. Consequently, at a  
590 concentration over 0.1 wt.% asphaltene, the layer consolidates. We hypothesize that  
591 after the 3D film is formed the film thickness increases, thus showing a stabilizing effect  
592 of interfacial layers when emulsions are formed [28,29].

593



594  
595 **Figure 9.** Interfacial dilational rheology of decalin with asphaltene content (rising drop)  
596 in surrogate bio-oil at 0.02 – 1 wt.% asphaltenes. Left: Dynamic interfacial tension at 3  
597 min observation as a function of asphaltene content. Right: Dilational modulus (E) at 3  
598 min observation as a function of asphaltene content. Measurements were performed  
599 with oscillation at a constant frequency of 0.1 Hz. T=20 ± 2 °C.

600

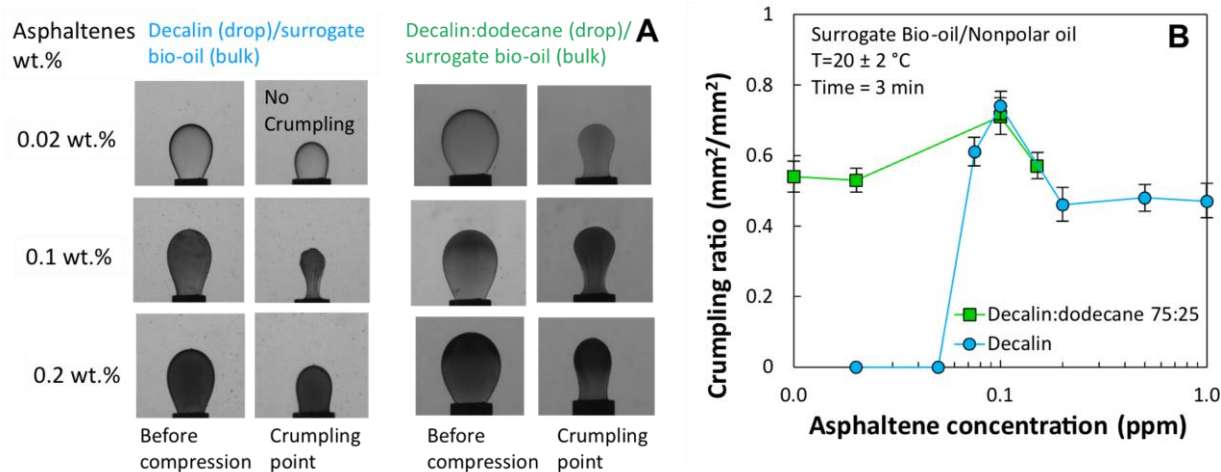
### 601 3.3.3 Crumpling ratio of surrogate bio-oil / oil interfaces

602 Figure 10 presents the crumpling ratios of decalin and decaline:dodecane 75:25 with  
603 varying asphaltene content (rising drop) in a surrogate bio-oil (bulk) wt.% for the case of  
604 decalin as solvent medium. No crumpling or "skin" formation is observed at 0.02 % and  
605 0.05 % asphaltenes. This may be attributed to the low concentration of asphaltenes and  
606 the suitability of decalin solvent to disperse them, not generating large asphaltene  
607 aggregates that could adsorb at the interface. Consequently, higher asphaltene  
608 concentrations are needed to form a solid-like interfacial layer. The crumpling ratio  
609 measured is maximum at 0.1 wt.% asphaltenes, which confirms the previous interfacial  
610 dilational rheology result. This validates the hypothesis that an elastic, solid-like  
611 asphaltene film with high mechanical resistance could be responsible for the high  
612 stability of bio-oil in oil emulsions with asphaltene content. The evolution of the

613 crumpling ratio with increasing asphaltene concentration is shown in Figure 10 right  
614 panel, with a maximum crumpling ratio attained at 0.1 wt.% asphaltenes.

615  
616 In the scenario of decalin:dodecane as non-polar oil, the crumpling ratio can be  
617 measured starting at 0.01 wt.% asphaltenes, indicating that the addition of dodecane to  
618 the system increases the asphaltenes interfacial activity, thus forming an interfacial film  
619 that ages rapidly and generates the so-called “skin”. A maximum crumpling ratio is  
620 shown again at 0.1 wt.% asphaltenes, confirming the elastic modulus maximum  
621 presented in Figure 9.

622  
623



624 **Figure 10.** A) Oil droplet in surrogate bio-oil before compression and at the crumpling  
625 point. B) Crumpling ratio of decalin and decalin:dodecane 75:25 with asphaltene content  
626 (rising drop) in surrogate bio-oil at 0.02 – 0.12 wt.% asphaltenes. The crumpling ratio  
627 was measured with a 1 μL oil drop, which is compressed after 3 min, at a constant  
628 volume rate (0.1 μL/s). T=20 ± 2 °C.

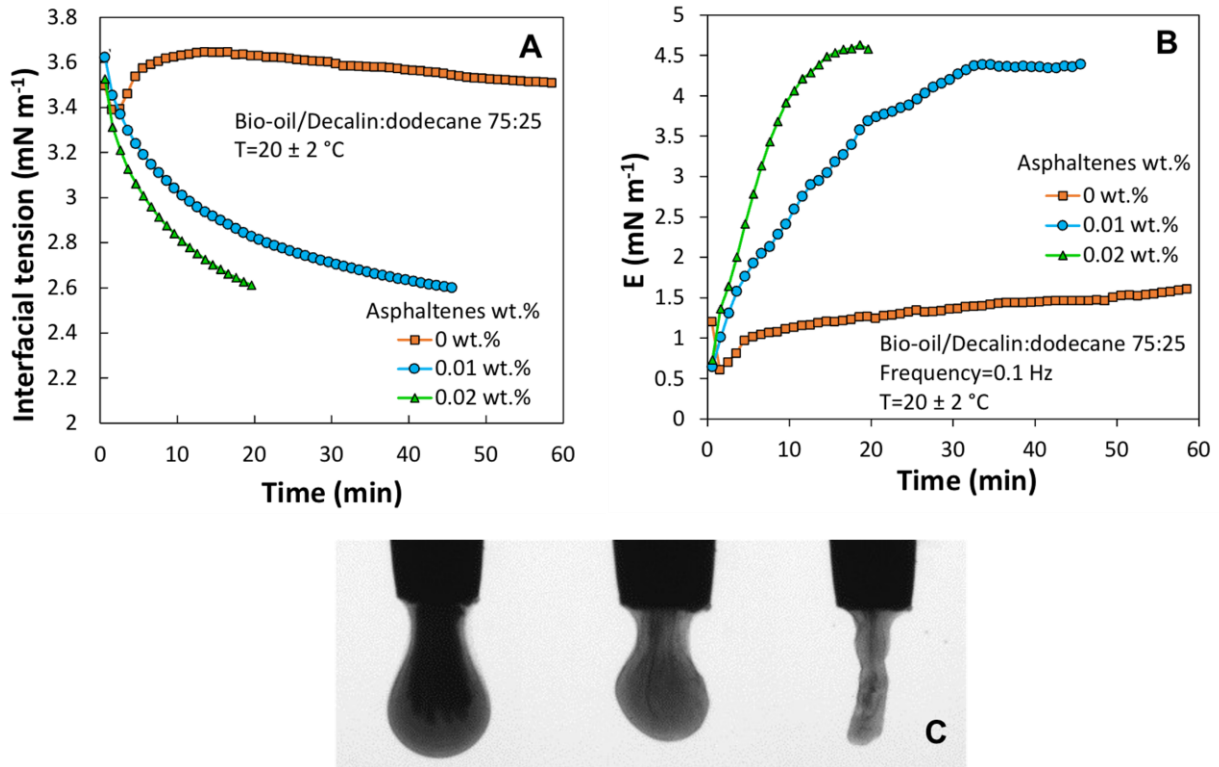
### 631 3.4 Interfacial properties of asphaltene/wood pyrolysis bio-oil/ model 632 hydrocarbon system

633  
634 In order to verify the results obtained with a surrogate pyrolysis oil, in this last section,  
635 the rheology of real wood pyrolysis bio-oil/petroleum-derived oil interfacial layers was  
636 measured at various asphaltene concentrations. There are several challenges related to  
637 the measurement of these systems, mainly that hydrocarbon oils with asphaltene  
638 content are black and wood pyrolysis are dark brown. Therefore, the observation with  
639 drop profile technique is not possible, unless very low asphaltene concentrations are  
640 used. For this reason, a model hydrocarbon phase (decalin:dodecane 75:25) with low  
641 asphaltene content was used as surrounding phase and a pendant drop of real bio-oil  
642 (which is denser) was formed. Bio-oils are complex mixtures, including lignin oligomers  
643 that could have some interfacial activity (which could be low according to Figure S3 in  
644 supplementary information). Constantino et al. indicate that lignin assumes a three-  
645 dimensional arrangement even within a single layer after adsorption at the interface  
646 [73].

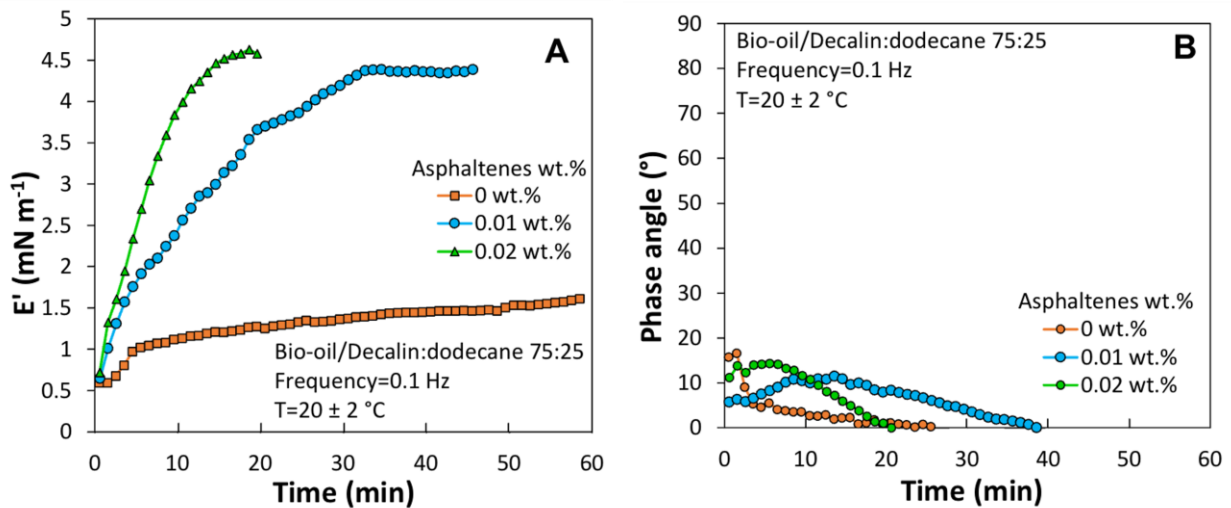
647  
648 Figure 11A shows the variation of the interfacial tension as a function of the ageing time  
649 of the bio-oil/petroleum-based oil interface. In the absence of asphaltenes, the  
650 interfacial tension remains with no visible variation in 60 min (around 3.6 mN/m),  
651 suggesting that bio-oil contains a low quantity of species with interfacial activity.  
652 However, the interfacial tension is much lower when compared to water/petroleum-  
653 based oil systems, which might be reasonable given an interface between two oils. In  
654 contrast, when 0.02 wt.% asphaltenes are added to the petroleum-based oil, there is a  
655 continuous interfacial tension decrease (from 3.6 to 2.6 mN/m in 45 min), indicating  
656 significant asphaltene interfacial activity at this concentration, after the 0.01 wt.%  
657 threshold has been reached.

658 The dilational modulus evolves as a function of time, evidencing the consolidation of the  
659 interface (Figure 12 and 13). The interfacial tensions measured for this system are in  
660 the range of 1 to 3 mN/m, which can be considered at the lower limit for the utilization of  
661 the pendant drop equipment.

662 When the dilational elasticity of the three systems at 0, 0.01 and 0.02 wt.% asphaltenes  
663 is compared in Figure 11B (measurements performed at a 0.1 Hz oscillation frequency),  
664 the effect of the asphaltene adsorption in the interfacial layer is clear. The system  
665 without asphaltenes shows a slight increase in the dilational modulus  $E$ , which is around  
666 1.1 mN/m. Moreover, when the asphaltene content is increased to 0.01 and 0.02 wt.%,  
667  $E$  increases at least four times in comparison to the 0 % asphaltene case. This can be  
668 observed in Figure 12, where the elastic modulus  $E'$  increases over time, indicating the  
669 formation of an elastic and high mechanical resistance interfacial film. This layer forms  
670 due to the adsorption of asphaltene aggregates and the consolidation of the layer as a  
671 function of time. Phase angle is reported in Figure 12B, which is low even for the 0 %  
672 asphaltene case, indicating that although  $E$  is low, bio-oil components seem to generate  
673 a low phase angle. The latter could create a synergy with asphaltenes to form such a  
674 solid-like layer as the interface ages, though this needs further confirmation. The  
675 formation of the solid-like layer at the interface is confirmed in Figure 11C, where the  
676 bio-oil droplet in the 0.02 wt.% asphaltene system is subjected to a retraction in volume  
677 with a crumpling ratio-like measurement, indicating the formation of a consolidated  
678 solid-like layer, similarly to water/crude oil systems [28,74,75].  
679



680  
 681 **Figure 11.** Interfacial dilational rheology of bio-oil (pendant drop) in decalin:dodecane  
 682 75:25 mixtures at 0, 0.1 and 0.2 wt.% asphaltenes. A) Dynamic interfacial tension. B) Dilational  
 683 modulus obtained with oscillatory measurements at constant frequency of 0.1 Hz. C) Progression of the wood  
 684 pyrolysis bio-oil pendant drop at 0.02 wt.% asphaltenes in decalin:dodecane 75:25 mixtures as a function  
 685 of the droplet compression at a 0.1  $\mu\text{L/s}$  rate. A viscoelastic film or “skin” is formed which is evidenced  
 686 when the total volume of the bio-oil is suctioned by the needle.  $T=20 \pm 2 \text{ }^\circ\text{C}$ . In the latter case the  
 687 measurements are shown for 20 minutes because at larger times a non-Laplacian shape was attained,  
 688 and  $E$  measurement under oscillation could not be performed.  
 689  
 690  
 691





693 **Figure 12.** Interfacial dilational rheology of bio-oil (pendant drop) in decalin:dodecane  
694 75:25 mixtures at 0, 0.01 and 0.02 wt.% asphaltenes. A) Evolution of the elastic  
695 modulus ( $E'$ ) as a function of time. B) Phase angle ( $\varphi$ ) as a function of time.  
696 Measurements were obtained with oscillatory measurements at constant frequency of  
697 0.1 Hz.  $T=20 \pm 2^\circ\text{C}$ . At 0.02 wt.% asphaltenes the measurements are shown for 20  
698 minutes because at larger times a non-Laplacian shape was attained, and E  
699 measurement under oscillation could not be performed.

700  
701 The previous results were obtained at an oscillation frequency of 0.1 Hz. In order to  
702 verify that asphaltenes' effect on the rheology of interfacial layers in a bio-oil/petroleum-  
703 based oil system is similar when compared to water/petroleum-based oil systems, an  
704 interfacial rheology frequency sweep was performed from 0.025 to 0.25 Hz. In Figure  
705 S4 (Supplementary information), frequency sweeps of the bio-oil (pendant  
706 drop)/decalin:dodecane (75:25) system at 0 and 0.01 wt.% asphaltenes is presented.  
707 Thus, it is proved that the asphaltene interfacial layers at a bio-oil/petroleum-based oil  
708 interface generate a solid-like behaviour when the frequency is increased. This is shown  
709 with two parameters, firstly, the increase in E as a function of the oscillation frequency  
710 of the droplet's interfacial area, and secondly, the decrease in phase angle. At a  
711 frequency of 0.25 Hz the phase angle of the bio-oil/petroleum-based oil with asphaltene  
712 content reaches a value below 5 degrees, indicative of a solid-like interface. It is  
713 important to note that the frequency sweep of the 0.02 wt.% asphaltenes system is not  
714 shown in Figure S3 because it developed a "skin"-like interface very fast with a low  
715 interfacial tension. Thus, the droplet developed a non-Laplacian shape and additionally  
716 it detached from the needle when it reached low interfacial tension. Also, it should be  
717 mentioned that systems with higher asphaltene content could not be measured due to  
718 the opacity of the petroleum-based oil at 0.04 wt.% asphaltenes.

#### 719 720 **4. Conclusions**

721  
722 In this work, bio-oil/oil interfaces are studied and the importance of asphaltene  
723 concentration in stabilizing bio-oil-in-oil emulsions is presented. The stabilization of  
724 surrogate wood pyrolysis oil-in-hydrocarbon (decalin or decaline:dodecane mixture)  
725 emulsions using asphaltenes requires a minimum concentration of 0.2 wt.%  
726 asphaltenes. The addition of dodecane to decalin shows that increasing the paraffinic  
727 content of the hydrocarbon phase improves bio-oil-in-oil emulsion stability.

728  
729 Interfacial rheology measurements prove effective to study the interfacial layer of bio-  
730 oil/petroleum-derived oils with asphaltene content, revealing a consolidation of the layer  
731 and the formation of a solid-like film when asphaltene content is increased. However,  
732 limitations exist when working with opaque phases such as bio-oils and fuels. To  
733 overcome this challenge, the use of surrogate bio-oils or model hydrocarbon phases  
734 can provide translucent phases, enabling pendant drop or rising drop configurations to be  
735 used for further studies.

736  
737 Asphaltenes form a solid-like interfacial layer evidenced by the increase in the dilational  
738 modulus ( $E$ ), leading to the formation of a stable, three-dimensional film at 0.1 wt.%

739 asphaltenes. A particularly low interfacial tension was found in bio-oil/petroleum-based  
740 oil interfaces (1-2 mN/m) when compared to water/oil systems. Asphaltenes layers that  
741 are formed at bio-oil/oil interfaces showed a decrease in interfacial tension as a function  
742 of concentration. The dilational modulus (E) is maximum at a concentration below this  
743 point. Once the maximum E is reached, the surface layer collapses and forms  
744 structures in three dimensions. Consequently, the interfacial layer presents a low  
745 resistance to compression, and E decreases [28,70].

746  
747 The use of native surfactants from petroleum facilitates the formulation of wood  
748 pyrolysis oil-in fuel emulsions. This work contributes to the understanding of the  
749 dynamics of bio-oil/oil interfaces, with applications in marine fuels and for refinery co-  
750 processing. The goal is to decrease the carbon footprint of fuels by incorporating a  
751 biogenic fuel source, such as wood pyrolysis oils.

752

### 753 **Acknowledgements**

754 The authors would like to thank TotalEnergies for financing this work and for allowing its  
755 publication. Chevreul Institute (FR 2638), Ministère de l'Enseignement Supérieur et de  
756 la Recherche, Région Nord-Pas de Calais and FEDER are also acknowledged for  
757 supporting this work. We would also like to thank Dominique Langevin, Jean-Marie  
758 Aubry, Maurice Bourrel and Nicolas Passade-Boupat for the helping discussions on  
759 emulsions and interfaces.

760

### 761 **References**

- 762 [1] A. Oasmaa, J. Lehto, Y. Solantausta, S. Kallio, Historical Review on VTT Fast Pyrolysis Bio-oil  
763 Production and Upgrading, *Energy Fuels* 35 (2021) 5683–5695.  
764 <https://doi.org/10.1021/acs.energyfuels.1c00177>.
- 765 [2] F. D.F. Chuahy, C.E.A. Finney, B.C. Kaul, M.D. Kass, Computational exploration of bio-oil blend  
766 effects on large two-stroke marine engines, *Fuel* 322 (2022) 123977.  
767 <https://doi.org/10.1016/j.fuel.2022.123977>.
- 768 [3] C. Lindfors, D.C. Elliott, W. Prins, A. Oasmaa, J. Lehtonen, Co-processing of Biocrudes in Oil  
769 Refineries, *Energy Fuels* (2022). <https://doi.org/10.1021/acs.energyfuels.2c04238>.
- 770 [4] A. de R. Pinho, M.B.B. de Almeida, F.L. Mendes, V.L. Ximenes, L.C. Casavechia, Co-processing raw  
771 bio-oil and gasoil in an FCC Unit, *Fuel Process. Technol.* 131 (2015) 159–166.  
772 <https://doi.org/10.1016/j.fuproc.2014.11.008>.
- 773 [5] Asmaa.A.M. Ali, Mustafa.A. Mustafa, K.E. Yassin, A techno-economic evaluation of bio-oil co-  
774 processing within a petroleum refinery, *Biofuels* 12 (2021) 1–9.  
775 <https://doi.org/10.1080/17597269.2018.1519758>.
- 776 [6] T. Janosik, A.N. Nilsson, A.C. Hällgren, M. Hedberg, C. Bernlind, H. Rådberg, L. Ahlsén, P. Arora,  
777 O.G.W. Öhrman, Derivatizing of Fast Pyrolysis Bio-Oil and Coprocessing in Fixed Bed Hydrotreater,  
778 *Energy Fuels* 36 (2022) 8274–8287. <https://doi.org/10.1021/acs.energyfuels.2c01608>.
- 779 [7] A. Oasmaa, T. Sundqvist, E. Kuoppala, M. Garcia-Perez, Y. Solantausta, C. Lindfors, V. Paasikallio,  
780 Controlling the phase stability of biomass fast pyrolysis bio-oils, *Energy Fuels* 29 (2015) 4373–4381.  
781 <https://doi.org/10.1021/acs.energyfuels.5b00607>.
- 782 [8] J. Cai, M.M.M. Rahman, S. Zhang, M. Sarker, X. Zhang, Y. Zhang, X. Yu, E.H. Fini, Review on Aging of  
783 Bio-Oil from Biomass Pyrolysis and Strategy to Slowing Aging, *Energy Fuels* 35 (2021) 11665–  
784 11692. <https://doi.org/10.1021/acs.energyfuels.1c01214>.



- 785 [9] A. Oasmaa, I. Fonts, M.R. Pelaez-Samaniego, M. Garcia-Perez, M. Garcia-Perez, Pyrolysis Oil  
786 Multiphase Behavior and Phase Stability: A Review, *Energy Fuels* 30 (2016) 6179–6200.  
787 <https://doi.org/10.1021/acs.energyfuels.6b01287>.
- 788 [10] X. Yuan, X. Ding, L. Leng, H. Li, J. Shao, Y. Qian, H. Huang, X. Chen, G. Zeng, Applications of bio-oil-  
789 based emulsions in a DI diesel engine: The effects of bio-oil compositions on engine performance  
790 and emissions, *Energy* 154 (2018) 110–118. <https://doi.org/10.1016/j.energy.2018.04.118>.
- 791 [11] X.L. Wang, X.Z. Yuan, H.J. Huang, L.J. Leng, H. Li, X. Peng, H. Wang, Y. Liu, G.M. Zeng, Study on the  
792 solubilization capacity of bio-oil in diesel by microemulsion technology with Span80 as surfactant,  
793 *Fuel Process. Technol.* 118 (2014) 141–147. <https://doi.org/10.1016/j.fuproc.2013.08.020>.
- 794 [12] A. Zia, E. Pentzer, S. Thickett, K. Kempe, Advances and Opportunities of Oil-in-Oil Emulsions, *ACS*  
795 *Appl. Mater. Interfaces* 12 (2020) 38845–38861. <https://doi.org/10.1021/acsami.0c07993>.
- 796 [13] X. Lu, J.S. Katz, A.K. Schmitt, J.S. Moore, A Robust Oil-in-Oil Emulsion for the Nonaqueous  
797 Encapsulation of Hydrophilic Payloads, *J. Am. Chem. Soc.* 140 (2018) 3619–3625.  
798 <https://doi.org/10.1021/jacs.7b11847>.
- 799 [14] A. Imhof, D.J. Pine, Stability of nonaqueous emulsions, *J. Colloid Interface Sci.* 192 (1997) 368–374.  
800 <https://doi.org/10.1006/jcis.1997.5020>.
- 801 [15] D. Crespy, K. Landfester, Making dry fertile: a practical tour of non-aqueous emulsions and  
802 miniemulsions, their preparation and some applications, *Soft Matter* 7 (2011) 11054–11064.  
803 <https://doi.org/10.1039/C1SM06156A>.
- 804 [16] L. Leng, H. Li, X. Yuan, W. Zhou, H. Huang, Bio-oil upgrading by emulsification/microemulsification:  
805 A review, *Energy* 161 (2018) 214–232. <https://doi.org/10.1016/j.energy.2018.07.117>.
- 806 [17] M. Zhang, H. Wu, Stability of emulsion fuels prepared from fast pyrolysis bio-oil and glycerol, *Fuel*  
807 206 (2017) 230–238. <https://doi.org/10.1016/j.fuel.2017.06.010>.
- 808 [18] D. Chiamonti, M. Bonini, E. Fratini, G. Tondi, K. Gartner, A. V. Bridgwater, H.P. Grimm, I. Soldaini,  
809 A. Webster, P. Baglioni, Development of emulsions from biomass pyrolysis liquid and diesel and  
810 their use in engines - Part 1: Emulsion production, *Biomass Bioenergy* 25 (2003) 85–99.  
811 [https://doi.org/10.1016/S0961-9534\(02\)00183-6](https://doi.org/10.1016/S0961-9534(02)00183-6).
- 812 [19] M.D.G. de Luna, L.A.D. Cruz, W.-H.H. Chen, B.-J.J. Lin, T.-H.H. Hsieh, Improving the stability of  
813 diesel emulsions with high pyrolysis bio-oil content by alcohol co-surfactants and high shear mixing  
814 strategies, *Energy* 141 (2017) 1416–1428. <https://doi.org/10.1016/j.energy.2017.11.055>.
- 815 [20] B.J. Lin, W.H. Chen, W.M. Budzianowski, C.T. Hsieh, P.H. Lin, Emulsification analysis of bio-oil and  
816 diesel under various combinations of emulsifiers, *Appl. Energy* 178 (2016) 746–757.  
817 <https://doi.org/10.1016/j.apenergy.2016.06.104>.
- 818 [21] Y.-K. Park, J.-M. Ha, S. Oh, J. Lee, Bio-oil upgrading through hydrogen transfer reactions in  
819 supercritical solvents, *Chem. Eng. J.* 404 (2021) 126527.  
820 <https://doi.org/10.1016/j.cej.2020.126527>.
- 821 [22] A. Dimitriadis, D. Liakos, U. Pfisterer, M. Moustaka-Gouni, D. Karonis, S. Bezergianni, Impact of  
822 hydrogenation on miscibility of fast pyrolysis bio-oil with refinery fractions towards bio-oil refinery  
823 integration, *Biomass Bioenergy* 151 (2021) 106171.  
824 <https://doi.org/10.1016/j.biombioe.2021.106171>.
- 825 [23] S. Nanda, F. Pattnaik, V.B. Borugadda, A.K. Dalai, J.A. Kozinski, S. Naik, Catalytic and Noncatalytic  
826 Upgrading of Bio-Oil to Synthetic Fuels: An Introductory Review, *ACS Symp. Ser.* 1379 (2021) 1–28.  
827 <https://doi.org/10.1021/bk-2021-1379.ch001>.
- 828 [24] P. Prasertpong, N. Tippayawong, Upgrading of biomass pyrolysis oil model compound via  
829 esterification: Kinetic study using heteropoly acid, *Energy Procedia* 160 (2019) 253–259.  
830 <https://doi.org/10.1016/j.egypro.2019.02.144>.

- 831 [25] X. Hu, R. Gunawan, D. Mourant, M.D.M. Hasan, L. Wu, Y. Song, C. Lievens, C.Z. Li, Upgrading of bio-  
832 oil via acid-catalyzed reactions in alcohols — A mini review, *Fuel Process. Technol.* 155 (2017) 2–  
833 19. <https://doi.org/10.1016/j.fuproc.2016.08.020>.
- 834 [26] M. Gradzielski, D. Langevin, B. Farago, Experimental investigation of the structure of nonionic  
835 microemulsions and their relation to the bending elasticity of the amphiphilic film, *Phys. Rev. E* 53  
836 (1996) 3900. <https://doi.org/10.1103/PhysRevE.53.3900>.
- 837 [27] D. Langevin, Rheology of adsorbed surfactant monolayers at fluid surfaces, *Annu. Rev. Fluid Mech.*  
838 46 (2014) 47–65. <https://doi.org/10.1146/annurev-fluid-010313-141403>.
- 839 [28] G. Alvarez, S. Poteau, J.-F. Argillier, D. Langevin, J.-L. Salager, Heavy oil– water interfacial  
840 properties and emulsion stability: Influence of dilution, *Energy Fuels* 23 (2009) 294–299.  
841 <https://doi.org/10.1021/ef800545k>.
- 842 [29] C. Dicharry, D. Arla, A. Siquin, A. Graciaa, P. Bouriat, Stability of water/crude oil emulsions based  
843 on interfacial dilatational rheology, *J. Colloid Interface Sci.* 297 (2006) 785–791.  
844 <https://doi.org/10.1016/j.cocis.2014.08.003>.
- 845 [30] R. Marquez, A.M. Forgiarini, D. Langevin, J.-L. Salager, Instability of Emulsions Made with  
846 Surfactant–Oil–Water Systems at Optimum Formulation with Ultralow Interfacial Tension,  
847 *Langmuir* 34 (2018) 9252–9263. <https://doi.org/10.1021/acs.langmuir.8b01376>.
- 848 [31] R. Marquez, A.M. Forgiarini, D. Langevin, J.-L.J.-L. Salager, A. M. Forgiarini, D. Langevin, J.-L.J.-L.  
849 Salager, A.M. Forgiarini, D. Langevin, J.-L.J.-L. Salager, Breaking of Water-In-Crude Oil Emulsions.  
850 Part 9. New Interfacial Rheology Characteristics Measured Using a Spinning Drop Rheometer at  
851 Optimum Formulation, *Energy Fuels* 33 (2019) 8151–8164.  
852 <https://doi.org/10.1021/acs.energyfuels.9b01476>.
- 853 [32] J.M. Zamora, R. Marquez, A. Forgiarini, D. Langevin, J.-L. Salager, Interfacial rheology of low  
854 interfacial tension systems using a new oscillating spinning drop method, *J. Colloid Interface Sci.*  
855 519 (2018) 27–37. <https://doi.org/10.1016/j.jcis.2018.02.015>.
- 856 [33] M. Karbaschi, M. Lotfi, J. Krägel, A. Javadi, D. Bastani, R. Miller, Rheology of interfacial layers, *Curr.*  
857 *Opin. Colloid Interface Sci.* 19 (2014) 514–519. <https://doi.org/10.1016/j.cocis.2014.08.003>.
- 858 [34] M. Bourrel, R.S. Schechter, *Microemulsions and related systems: formulation, solvency, and*  
859 *physical properties*, 2nd ed., Editions Technip, Paris, France, Paris, France, 2010.
- 860 [35] R. Marquez, N. Acevedo, M. Rondon, A. Graciaa, J.-L. Daridon, J.-L. Salager, M. Rondón, A. Graciaa,  
861 J.-L. Daridon, J.-L. Salager, Breaking of Water-in-Crude Oil Emulsions. 10. Experimental Evidence  
862 from a Quartz Crystal Resonator Sensor and an Oscillating Spinning Drop Interfacial Rheometer,  
863 *Energy Fuels* 37 (2023) 2735–2749. <https://doi.org/10.1021/acs.energyfuels.2c03717>.
- 864 [36] M. Bourrel, N. Passade-Boupat, *Crude Oil Surface Active Species: Consequences for Enhanced Oil*  
865 *Recovery and Emulsion Stability*, *Energy Fuels* 32 (2018) 2642–2652.  
866 <https://doi.org/10.1021/acs.energyfuels.7b02811>.
- 867 [37] M. Jeribi, B. Almir-Assad, D. Langevin, I. Henaut, J.F. Argillier, Adsorption kinetics of asphaltenes at  
868 liquid interfaces, *J. Colloid Interface Sci.* 256 (2002) 268–272.  
869 <https://doi.org/10.1006/jcis.2002.8660>.
- 870 [38] E. Freer, K.S. Yim, G.G. Fuller, C.J. Radke, Interfacial rheology of globular and flexible proteins at  
871 the hexadecane/water interface: comparison of shear and dilatation deformation, *J. Phys. Chem. B*  
872 108 (2004) 3835–3844. <https://doi.org/10.1021/jp037236k>.
- 873 [39] N. Aske, R. Orr, J. Sjöblom, H. Kallevik, G. Øye, Interfacial properties of water–crude oil systems  
874 using the oscillating pendant drop. Correlations to asphaltene solubility by near infrared  
875 spectroscopy, *J. Dispers. Sci. Technol.* 25 (2004) 263–275. <https://doi.org/10.1081/DIS-120037694>.
- 876 [40] E.M. Freer, C.J. Radke, Relaxation of asphaltenes at the toluene/water interface: Diffusion  
877 exchange and surface rearrangement, *J. Adhes.* 80 (2004) 481–496.  
878 <https://doi.org/10.1080/00218460490477143>.

- 879 [41] M.A. Bos, T. Van Vliet, Interfacial rheological properties of adsorbed protein layers and surfactants:  
880 a review, *Adv. Colloid Interface Sci.* 91 (2001) 437–471. <https://doi.org/10.1016/S0001->  
881 8686(00)00077-4.
- 882 [42] R. Miller, J.K. Ferri, A. Javadi, J. Krägel, N. Mucic, R. Wüstneck, Rheology of interfacial layers,  
883 *Colloid Polym. Sci.* 288 (2010) 937–950.
- 884 [43] H.W. Yarranton, P. Urrutia, D.M. Sztukowski, Effect of interfacial rheology on model emulsion  
885 coalescence. II. Emulsion coalescence, *J. Colloid Interface Sci.* 310 (2007) 253–259.  
886 <https://doi.org/10.1016/j.jcis.2007.01.098>.
- 887 [44] H.W. Yarranton, D.M. Sztukowski, P. Urrutia, Effect of interfacial rheology on model emulsion  
888 coalescence. I. Interfacial rheology, *J. Colloid Interface Sci.* 310 (2007) 246–252.  
889 <https://doi.org/10.1016/j.jcis.2007.01.071>.
- 890 [45] H. Alboudwarej, J. Beck, W.Y. Svrcek, H.W. Yarranton, K. Akbarzadeh, Sensitivity of asphaltene  
891 properties to separation techniques, *Energy Fuels* 16 (2002) 462–469.  
892 <https://doi.org/10.1021/ef010213p>.
- 893 [46] C. Mase, R. Moulian, E. Lazzari, C. Garnier, M. Piparo, M. Hubert-Roux, C. Afonso, D.C. Dayton, C.  
894 Barrère-Mangote, P. Giusti, Comparison of lignocellulosic-based biomass pyrolysis processes by  
895 multi-scale molecular characterization, *J. Anal. Appl. Pyrolysis* 177 (2024) 106354.  
896 <https://doi.org/10.1016/j.jaap.2024.106354>.
- 897 [47] I. Fonts, M. Atienza-Martínez, H.-H.H. Carstensen, M. Benés, A.P.P. Pires, M. Garcia-Perez, R.  
898 Bilbao, Thermodynamic and Physical Property Estimation of Compounds Derived from the Fast  
899 Pyrolysis of Lignocellulosic Materials, *Energy Fuels* (2021).  
900 <https://doi.org/10.1021/acs.energyfuels.1c01709>.
- 901 [48] N. Muro-Suñé, G.M. Kontogeorgis, N. von Solms, M.L. Michelsen, Phase Equilibrium Modelling for  
902 Mixtures with Acetic Acid Using an Association Equation of State, *Ind. Eng. Chem. Res.* 47 (2008)  
903 5660–5668. <https://doi.org/10.1021/ie071205k>.
- 904 [49] G. Lemahieu, J. Le Maître, C. Mase, J. Maillard, J.F. Ontiveros, L. Ligiero, M. Loriau, P. Giusti, C.  
905 Afonso, J.-M. Aubry, V. Molinier, Extraction of Crude Oil Endogenous Surfactants by an Optimum  
906 Three-Phase Microemulsion System: Relation between Interfacial Behavior and a Molecular  
907 Fingerprint Obtained by Ultrahigh-Resolution Mass Spectrometry, *Energy Fuels* (2021).  
908 <https://doi.org/10.1021/acs.energyfuels.1c02524>.
- 909 [50] V.J. Verruto, P.K. Kilpatrick, Preferential solvent partitioning within asphaltenic aggregates  
910 dissolved in binary solvent mixtures, *Energy Fuels* 21 (2007) 1217–1225.  
911 <https://doi.org/10.1021/ef060456n>.
- 912 [51] T. Morita, M. Morimoto, S. Shibuta, H. Imamura, H. Yamamoto, R.R. Tykwinski, D.E. Scott, J.M.  
913 Stryker, T. Suzuki, R. Tanaka, Disaggregation of Asphaltene Aggregates in Solutions Depending  
914 upon Affinity Indices of the Hansen Solubility Parameter Using Ultrasmall-, Small-, and Wide-Angle  
915 X-ray Scattering, *Energy Fuels* 36 (2022) 10043–10051.  
916 <https://doi.org/10.1021/acs.energyfuels.2c01668>.
- 917 [52] B. Creton, I. Lévêque, F. Oukhemanou, Equivalent alkane carbon number of crude oils: A predictive  
918 model based on machine learning, *Oil Gas Sci. Technol. – Rev. D'IFP Energ. Nouv.* 74 (2019) 30.  
919 <https://doi.org/10.2516/ogst/2019002>.
- 920 [53] S.H. Jang, G.A. Pope, Microemulsion phase behavior of live crude oil and revisiting the EACN  
921 framework for crude oils, *Colloids Surf. Physicochem. Eng. Asp.* 670 (2023) 131565.  
922 <https://doi.org/10.1016/j.colsurfa.2023.131565>.
- 923 [54] L. Chang, G.A. Pope, S.H. Jang, M. Tagavifar, Prediction of microemulsion phase behavior from  
924 surfactant and co-solvent structures, *Fuel* 237 (2019) 494–514.  
925 <https://doi.org/10.1016/j.fuel.2018.09.151>.

- 926 [55] L. Delforce, E. Hofmann, V. Nardello-Rataj, J.-M. Aubry, TiO<sub>2</sub> nanoparticle dispersions in water and  
927 nonaqueous solvents studied by gravitational sedimentation analysis: Complementarity of Hansen  
928 Parameters and DLVO interpretations, *Colloids Surf. Physicochem. Eng. Asp.* 628 (2021) 127333.  
929 <https://doi.org/10.1016/j.colsurfa.2021.127333>.
- 930 [56] A. Hemmati-Sarapardeh, B. Dabir, M. Ahmadi, A.H. Mohammadi, M.M. Husein, Toward  
931 mechanistic understanding of asphaltene aggregation behavior in toluene: The roles of asphaltene  
932 structure, aging time, temperature, and ultrasonic radiation, *J. Mol. Liq.* 264 (2018) 410–424.  
933 <https://doi.org/10.1016/j.molliq.2018.04.061>.
- 934 [57] S.D. Taylor, J. Czarnecki, J. Masliyah, Refractive index measurements of diluted bitumen solutions,  
935 *Fuel* 80 (2001) 2013–2018. [https://doi.org/10.1016/S0016-2361\(01\)00087-4](https://doi.org/10.1016/S0016-2361(01)00087-4).
- 936 [58] A. Hutin, Application notes - Method: 1. Measurement of interfacial tension with pendant/rising  
937 drop method, (2019). [https://www.researchgate.net/publication/334203912\\_Application\\_Notes\\_-](https://www.researchgate.net/publication/334203912_Application_Notes_-_Method_1_Measurement_of_interfacial_tension_with_pendant_rising_drop_method)  
938 [Method\\_1\\_Measurement\\_of\\_interfacial\\_tension\\_with\\_pendant\\_rising\\_drop\\_method](https://www.researchgate.net/publication/334203912_Application_Notes_-_Method_1_Measurement_of_interfacial_tension_with_pendant_rising_drop_method) (accessed  
939 May 1, 2024).
- 940 [59] A. Hutin, M.S. Carvalho, Use of a Geometric Parameter for Characterizing Rigid Films at Oil–Water  
941 Interfaces, *Langmuir* 38 (2022) 10139–10149. <https://doi.org/10.1021/acs.langmuir.2c01058>.
- 942 [60] G. Loglio, P. Pandolfini, L. Liggieri, A. V. Makievski, F. Ravera, Determination of interfacial  
943 properties by the pendant drop tensiometry: Optimisation of experimental and calculation  
944 procedures, *Bubble Drop Interfaces* 2 (2011) 7–38. <https://doi.org/10.1201/b12177-4>.
- 945 [61] J.D. McLean, P.K. Kilpatrick, Effects of asphaltene solvency on stability of water-in-crude-oil  
946 emulsions, *J. Colloid Interface Sci.* 189 (1997) 242–253. <https://doi.org/10.1006/jcis.1997.4807>.
- 947 [62] T. Lukowicz, A. Benazzouz, V. Nardello-Rataj, J.M. Aubry, Rationalization and Prediction of the  
948 Equivalent Alkane Carbon Number (EACN) of Polar Hydrocarbon Oils with COSMO-RS  $\sigma$ -Moments,  
949 *Langmuir* 31 (2015) 11220–11226. <https://doi.org/10.1021/acs.langmuir.5b02545>.
- 950 [63] L. Meza, J.G. Alvarado, R. Marquez, A. Forgiarini, Demulsifier’s performance evaluation using the  
951 optimum formulation concept HLD. Practical case: Heavy crude-oil diluted in naphtha or in  
952 synthetic aromatic oil, *SPE J.* (2022).
- 953 [64] V.J. Verruto, P.K. Kilpatrick, Water-in-model oil emulsions studied by small-angle neutron  
954 scattering: Interfacial film thickness and composition, *Langmuir* 24 (2008) 12807–12822.  
955 <https://doi.org/10.1021/la802095m>.
- 956 [65] N. Passade-Boupat, H. Zhou, M. Rondon-Gonzalez, Asphaltene Precipitation from Crude Oils : How  
957 to Predict it and to Anticipate Treatment?, *SPE Middle East Oil Gas Show Conf.* 1 (2013) 394–402.  
958 <https://doi.org/10.2118/164184-MS>.
- 959 [66] C.R.E. Mansur, A.R. de Melo, E.F. Lucas, Determination of Asphaltene Particle Size: Influence of  
960 Flocculant, Additive, and Temperature, *Energy Fuels* 26 (2012) 4988–4994.  
961 <https://doi.org/10.1021/ef300365x>.
- 962 [67] S. Campen, B. Smith, J. Wong, Deposition of Asphaltene from Destabilized Dispersions in Heptane-  
963 Toluene, *Energy Fuels* 32 (2018) 9159–9171. <https://doi.org/10.1021/acs.energyfuels.8b01887>.
- 964 [68] J.-L. Bridot, D. Langevin, O.C. Mullins, Role of Asphaltene Origin in Its Adsorption at Oil–Water  
965 Interfaces, *Energy Fuels* 36 (2022) 8749–8759. <https://doi.org/10.1021/acs.energyfuels.2c00966>.
- 966 [69] O. Mullins, A. Pomerantz, Y. Zhang, Asphaltenes: Fundamental Principles to Oilfield Applications,  
967 *SPE Annu. Tech. Conf. Exhib.* (2021) 1–28. <https://doi.org/10.2118/206091-MS>.
- 968 [70] D. Langevin, *Emulsions, Microemulsions and Foams*, Springer, Gewerbestr, Switzerland, 2020.  
969 <https://doi.org/10.1007/978-3-030-55681-5>.
- 970 [71] L. Goual, G. Horváth-Szabó, J.H. Masliyah, Z. Xu, Adsorption of Bituminous Components at  
971 Oil/Water Interfaces Investigated by Quartz Crystal Microbalance: Implications to the Stability of  
972 Water-in-Oil Emulsions, *Langmuir* 21 (2005) 8278–8289. <https://doi.org/10.1021/la050333f>.

- 973 [72] G. Alvarez, J. Jestin, J.F. Argillier, D. Langevin, Small-Angle Neutron Scattering Study of Crude Oil  
974 Emulsions: Structure of the Oil–Water Interfaces, *Langmuir* 25 (2009) 3985–3990.  
975 <https://doi.org/10.1021/la802736c>.
- 976 [73] C.J.L. Constantino, L.P. Juliani, V.R. Botaro, D.T. Balogh, M.R. Pereira, E.A. Ticianelli, A.A.S.S.  
977 Curvelo, O.N. Oliveira, C.J.L. Constantino, L.P. Juliani, V.R. Botaro, D.T. Balogh, M.R. Pereira, E.A.  
978 Ticianelli, A.A.S.S. Curvelo, O.N. Oliveira, Langmuir-Blodgett films from lignins, *Thin Solid Films*  
979 284–285 (1996) 191–194. [https://doi.org/10.1016/S0040-6090\(95\)08303-0](https://doi.org/10.1016/S0040-6090(95)08303-0).
- 980 [74] S.L. Kokal, Crude Oil Emulsions: A State-Of-The-Art Review, *SPE Prod. Facil.* 20 (2005) 5–13.  
981 <https://doi.org/10.2118/77497-PA>.
- 982 [75] S. Gao, K. Moran, Z. Xu, J. Masliyah, Role of bitumen components in stabilizing water-in-diluted oil  
983 emulsions, *Energy Fuels* 23 (2009) 2606–2612. <https://doi.org/10.1021/ef801089c>.  
984  
985